Pharm Res (2014) 31:607–634
DOI 10.1007/s11095-013-1184-3

RESEARCH PAPER

In Vitro, In Vivo, and *In Silico* Evaluation of the Bioresponsive Behavior of an Intelligent Intraocular Implant

Lisa C. du Toit • Trevor Carmichael • Thirumala Govender • Pradeep Kumar • Yahya E. Choonara • Viness Pillay

Received: 2 May 2013 / Accepted: 9 August 2013 / Published online: 4 September 2013

ABSTRACT

Purpose An autofeedback complex polymeric platform was used in the design of an intelligent intraocular implant—the I^3—using stimuli-responsive polymers, producing a smart release system capable of delivering therapeutic levels of an anti-inflammatory agent (indomethacin) and antibiotic (ciprofloxacin) for posterior segment disorders of the eye in response to inflammation.

Methods Physicochemical and physicomechanical analysis of the I^3 was undertaken to explicate the highly crosslinked make-up and 'on-off' inflammation-responsive performance of the I^3. In addition, energetic profiles for important complexation reactions were generated using Molecular Mechanics Energy Relationships by exploring the spatial disposition of energy minimized molecular structures. Furthermore, preliminary *in vivo* determination of the inflammation-responsiveness of the I^3 was ascertained following implantation in the normal and inflamed rabbit eye.

Results *In silico* modeling simulating a pathological inflammatory intraocular state highlighted the interaction potential of hydroxyl radicals with the selected polysaccharides comprising the I^3. The intricately crosslinked polymeric system forming the I^3 thus responded at an innate level predicted by its molecular make-up to inflammatory conditions as indicated by the results of the drug release studies, rheological analysis, magnetic resonance imaging and scanning electron microscopic imaging. *In vivo* drug release analysis demonstrated indomethacin levels of 0.749 ± 0.126 μg/mL and 1.168 ± 0.186 μg/mL, and ciprofloxacin levels of 1.181 ± 0.150 μg/mL and 6.653 ± 0.605 μg/mL in the normal and inflamed eye, respectively.

Conclusions Extensive *in vitro*, molecular, and *in vivo* characterization therefore highlighted successful inflammation-responsiveness of the I^3. The I^3 is a proposed step forward from other described ocular systems owing to its combined bioresponsive, nano-enabled architecture.

KEY WORDS *in vivo* test · inflammation · intraocular implant · molecular modeling · physicochemical properties · physicomechanical properties · stimulus-responsive

ABBREVIATIONS

ALG	Alginate
BPMs	Bioresponsive polymeric matrices
CMV	Cytomegalovirus
DCC	*N*,*N*′-dicyclohexylcarbodiimide
DSPC	Distearoylphosphatidylcholine
DSPE	Distearoylphosphatidylethanolamine
HA	Hyaluronic acid
I^3	Intelligent Intraocular Implant
Lipo-CHT-PCL NS	Lipoidal-chitosan-poly(ε-caprolactone) nanosystem
LPS	Lipopolysaccharide
MMER	Molecular Mechanics Energy Relationships
NS	Nanosystem/s
OH	Hydroxyl radicals
PAA	Poly(acrylic acid)
PCL	Poly(ε-caprolactone)
SRHS	Stimulus-responsive hydrogel system
SVH	Simulated vitreous humor

Electronic supplementary material The online version of this article (doi:10.1007/s11095-013-1184-3) contains supplementary material, which is available to authorized users.

L. C. du Toit · P. Kumar · Y. E. Choonara · V. Pillay (✉)
Department of Pharmacy and Pharmacology, Faculty of Health Sciences
University of the Witwatersrand, 7 York Road
Parktown, 2193 Johannesburg, South Africa
e-mail: viness.pillay@wits.ac.za

T. Carmichael
Ophthalmology Division, Department of Neurosciences
Faculty of Health Sciences, University of the Witwatersrand
7 York Road, Parktown, 2193 Johannesburg, South Africa

T. Govender
Department of Pharmaceutical Sciences, School of Health Sciences
University of KwaZulu Natal University Road
Westville, 4000 Durban, South Africa

INTRODUCTION

Inflammatory posterior segment ocular (vitreoretinal) disorders, such as uveitis (which may be infectious or non-infectious), have been highlighted as the foremost contributors to visual impairment, and ultimately blindness (1,2). Research has been implicit in conveying that controlled polymeric drug delivery systems are essential for realizing a superlative pharmaceutical intervention, where effective bioactives are available for intraocular disease treatment. Furthermore, of current and pertinent interest is the incorporation of a two-way communication between the body and polymeric delivery platforms for the creation of systems that recognize a biochemical process pertaining to a disease and respond aptly via drug release (3,4). Barbu and co-workers (4) proposed that sustained drug delivery from biodegradable implants incorporating 'smart' materials, combining the capabilities of stimulus response and molecular recognition, could possess enhanced potential for posterior segment disorder management. Furthermore, a number of inflammatory ocular diseases are chronic and hence require prolonged drug therapy. Release of an inflammation-reducing agent in a fashion responsive to a stimulus e.g. the presence of inflammatory reactions, would purportedly minimize adverse reactions related to the drug. Extrapolating current research on inflammation-responsive systems (5), design of a controlled release ocular delivery system that delivers an anti-inflammatory drug and possibly an antibiotic at a rate that is responsive to the presence or absence of inflammation in a patient on a specific day, for instance, would be particularly advantageous for the effective treatment of posterior segment disorders.

The current market leader representing intraocular implantable systems for the treatment of uveitis is Retisert™ incorporating a corticosteroid (fluocinolone 0.59 mg intravitreal implant, Bausch and Lomb, Inc.), the first FDA approved intravitreal implant for the treatment of chronic posterior non-infectious uveitis. The Retisert™ provides continuous delivery of the corticosteroid (6). Because there is uninterrupted release of anti-inflammatory drug, irrespective of alterations in the presence or absence of inflammation, there is an enhanced propensity for the occurrence of side effects, such as, cataract development, intraocular pressure elevation, procedural complications and eye pain (7). New developments in intraocular delivery systems have been reported (8–11). Their delivery mechanisms are generally based on attaining 'controlled and sustained' levels of drug (12). However, what must be kept in mind is that available intraocular implants for controlled high-dose corticosteroid delivery have suffered from a notably high complication rate, as highlighted during clinical trials conducted by Holekamp *et al*. (13). In terms of stimulus-responsive approaches employed in ocular drug delivery, Zeimer and Goldberg (14) have developed a method for local targeting of drugs in the eye based on a straightforward mechanism. The method, called light-targeted delivery (LTD), implicated the encapsulation of a drug in heat-sensitive liposomes, ensued with intravenous injection, and ultimate release of their content at the site of preference by non-invasively warming up the targeted tissue with a light pulse directed through the pupil of the eye (14). There is a scarcity of stimulus-responsive ocular systems, however, that exploit the intraocular inflammatory process. This begs the consideration of progressive and enhanced delivery system design strategies directed towards inflammation-responsiveness.

In this investigation, we therefore proposed the pragmatic design of an intelligent intraocular implant (I^3) that recognizes a specific biochemical process inherent to inflammation and then responds via an in-built mechanism to effect polymeric erosion with resultant drug release. Thus the platform on which the I^3 is based would incorporate potentially inflammation-responsive polymeric materials for implantable drug delivery. The premise is the design of inner and outer bioresponsive polymeric matrices (BPMs) that would erode and release an incorporated model anti-inflammatory and antibiotic in a fashion responsive to a stimulus, such as the highly reactive intermediates, including hydroxyl radicals ($OH^{\cdot}$), that are released from activated leukocytes both *in vitro* and during acute and chronic intraocular inflammatory reactions *in vivo* (15). Furthermore, the inner core is comprised of an anti-inflammatory agent encapsulated within a lipoidal-chitosan-poly(ε-caprolactone)-nanosystem (Lipo-CHT-PCL-NS). Erosion of the core in the presence of inflammation would result in release of the NS, which would target inflammatory sites. The configuration of the I^3 is such that it incorporated a model antibiotic, ciprofloxacin, in the outer BPM and model anti-inflammatory, indomethacin, in the inner BPM. The overall *modus operandi* of the I^3 is provided in Animation 1 (video) / Animation 1 *(still)*.

Hyaluronic acid (HA) was initially identified as the key polymer for formulation of the I^3 owing to its established inflammation-responsive capabilities. HA possesses a bioresorbable nature and ease of degradation *in vivo* due to the action of the enzyme hyaluronidase and free radicals, however, this ultimately restricts its use for applications where a more enduring effect is required. Thus, modification of HA while maintaining its bioresponisive potential was necessary so as to increase its residence lifetime and extend its potential applications (16). Additional inflammation-sensitive polymers were thus included together with HA to form a highly crosslinked, yet still innately inflammation-responsive implant. The proposed inflammation-sensitive polymers, together with HA, were formulated as multi-crosslinked simultaneously-originated BPMs possessing the inherent capabilities to meet the following design criteria:

1. Minimal drug release under *in vitro* conditions simulating a normal physiological intraocular state
2. Enhanced drug release (relative to the normal state) under *in vitro* conditions simulating a pathological inflammatory

intraocular state created in the presence of hydroxyl radicals generated via the Fenton reaction. A triggered erosion of the BPMs with a more rapid response from the outer BPM is necessitated for management of the initial infection and acute inflammatory response.

3. The inner (core) BPM should display modulated inflammation-responsive erosion to release the anti-inflammatory agent-loaded NS for management of the ensuing inflammation.
4. Correlation of *in vitro* behavior with *in vivo* performance in a suitable animal model with demonstration of a reduction in intraocular inflammation on release of the drug/s from the respective BPMs.

It is important to note that the I^3 is a proposed step forward from other described ocular systems owing to its combined bioresponsive nature and nano-based targeting capabilities, which would not provide sustained levels of drug for intraocular inflammatory condition-treatment (e.g. uveitis), but rather levels that are aligned with the presence or absence of intraocular inflammation experienced by a specific patient at a specific time, and therefore individualized and synchronized directly with the needs of the patient. Thus the described side effects that have been reported for products on the market would be minimized through the proposed system which would provide enhanced drug release when exposed to an inflammatory stimulus compared to when the implant is subjected to normal intraocular conditions. Furthermore, surgical complications (e.g. choroidal detachment, endophthalmitis, hypotony, retinal detachment, vitreous hemorrhage and/or loss, worsening of intraocular inflammation and wound dehiscence) (6) would be reduced in the I^3 due to the biodegradability of the device, obliterating the need for removal of the device which is necessitated in non-biodegradable ocular implants.

The interaction of the I^3 with the ocular environment is tantamount to elaboration of the bioresponsive capabilities of the device, which in turn depends on the characteristics of the device, and can be engineered into the implant by varying the chemical or physical properties of the polymer (17). Thus, interpretation of the physicochemical and physicomechanical properties is a prerequisite in defining the behavior/ performance of the device following implantation.

In silico modeling simulating a normal and a pathological inflammatory intraocular state (created in the presence of hydroxyl radicals) was initially performed to predict the effect of the inflammatory radicals on the selected polymers comprising the I^3, specifically the inflammation-responsive HA molecule. In order to gain an in-depth understanding of the crosslinking mechanisms employed to derive the device with rheological demonstration of pertinent transitions at the fabrication stage, consequent altered thermal and molecular vibrational behavior of the implant, and overall implant architecture; Fourier Transform-infrared spectroscopy, rheological investigations, Advanced Differential Scanning Calorimetric studies, and Scanning Electron Microscopy, were respectively and systematically performed. This was in tandem with drug release investigations and Magnetic Resonance Imaging explicating the on-off inflammation-responsive behavior of the I^3. These investigations would purportedly enable identification of the suitability of the I^3 as a bioresponsive system for potentially enhanced patient outcomes.

Ultimately the preliminary clinical potential of the I^3 in a rabbit eye model was assessed for its ability to respond with notably enhanced drug release when exposed to an inflammatory state—demonstration of the inflammation-responsive drug release could present a significant advance in the treatment of ocular inflammatory diseases and associated intraocular infections.

MATERIALS AND METHODS

Materials

For the Lipo-CHT-PCL Nanosystem

Chitosan (CHT, low molecular weight M_w < 6,000 Da, viscosity ~20 000cps), poly(ε-caprolactone) (PCL), indomethacin (99% TLC minimum), DL-α disteroylphosphatidylcholine (DSPC), L-α distearoylphosphatidylethanolimine methoxypolyethylene glycol conjugate (DSPE-mPEG, referred to as DSPE, henceforth), and Tween® 80 were all purchased from Sigma-Aldrich® Inc. (St. Louis, MO, USA). Acetone and hydrochloric acid (HCl, 32%) were obtained from Unilab (Merck Chemicals (Pty) Ltd, Wadeville, Gauteng). Chloroform spirit was purchased from Wako (Pure Chemical Industries, Ltd. Japan). All other reagents were of analytical grade and were used as received.

For the BPMs

Hyaluronic acid (potassium salt, from human umbilical cord), chitosan (MMW) *N*,*N*′-dicyclohexylcarbodiimide, indomethacin (99% TLC) and gluteraldehyde 25%$^{v}/_{v}$ were all purchased from Sigma-Aldrich® Inc. (St Louis, MO, USA). *N*-hydroxysuccimide and ciprofloxacin were purchased from Fluka® Analytical via Sigma-Aldrich® Inc. (St Louis, MO, USA). Alginate (TICA-algin® 400 Powder, medium viscosity) was purchased from Texture Innovation Center® (White Marsh, MD, USA). Other materials employed were polyacrylic acid (Carbopol 974P®) (Noveon Inc., Cleveland, Ohio, USA), as well as hydrochloric acid and aluminum chloride that were purchased from (Merck, Wadeville, Gauteng, South Africa). All other reagents were of analytical grade and used as received.

Synthetic Processes for I^3 Formulation

The I^3 was designed as a secure-fit dual bioresponsive polymeric matrix system with a NS enclatherated as a superlattice' with chitosan (CHT) forming the inner BPM in which the NS was embedded; and alginate (ALG), hyaluronic acid (HA) and poly(acrylic acid) (PAA) forming the inflammation-responsive outer BPM.

Synthesis of Lipoidal-Chitosan-Poly(ε-Caprolactone) Nanosystems

PCL (50 mg) and the anti-inflammatory, indomethacin (20 mg), were dissolved in 3 mL acetone. For the composite NS (Lipo-CHT-PCL NS), the phospholipids, DSPC (20 mg) and DSPE (5 mg), were dissolved in 2 mL chloroform and the organic phases mixed. Chitosan (low molecular weight, LMW) (50 mg) was dissolved in 15 mL 0.05 M HCl. Tween® 80 (0.01 mL) was included as a surfactant. The chitosan solution was slowly added to the phospholipid-PCL-indomethacin solution with sonication at a relative amplitude of 80 for 1 min (20 kHz sonicator, VibraCell, Sonics and Materials, Inc., Danbury, CT, USA). The organic solvent was subsequently evaporated with gentle stirring for 3 h. The interaction between the carboxyl or hydroxyl groups of the anionic PCL and the amine groups of chitosan formed immediate polyionic nanogels. The stability of the formed NS suspension was maintained through freezing at −80°C in an ultra-low freezer (Sanyo VIP™ Series, Sanyo North America Corporation, Wood Dale, IL, USA) prior to incorporation as the core of the I^3. The ultimate destination of the NS is incorporation within the core of the I^3, which would be composed of a crosslinked chitosan matrix. Chitosan (medium molecular weight, MMW) was hydrated in the NS suspension to yield a final MMW chitosan concentration of 13.33%$^{w}/_{v}$. This yielded the cationic polymer mixture for deriving the inner BPM of the I^3.

Formulation of the Bioresponsive Polymeric Matrices

For the outer BPM a 4%$^{w}/_{v}$ sodium alginate (ALG)—1%$^{w}/_{v}$ polyacrylic acid (PAA) (Carbopol® 974)—3%$^{w}/_{v}$ *N*—hydroxysuccimide (NHS)—0.25%w/v hyaluronic acid (HA)—2.5%$^{v}/_{v}$ gluteraldehyde—0.25%$^{w}/_{v}$ ciprofloxacin aqueous solution was prepared, instituting carbodiimide coupling chemistry to increase the interconnectivity of the matrix. *N*,*N*′-dicyclohexylcarbodiimide (DCC), which is commonly used as a coupling agent or activator, was employed to facilitate coupling between the HA and ALG, and the PAA. DCC (300 mg) was dissolved in ethanol and dispersed within the polymeric solution. This formed the anionic polymer-drug solution.

In this synthetic effort, the carbodiimide functionality acts as a dehydration agent and activates carboxylic acids towards amide or ester formation. The inclusion of additives or reagents in the polymeric composition, namely NHS, has the purpose of increasing the reaction yield, i.e., increasing interpolymeric crosslinking via, proposedly, amide formation, and decreasing side reactions (18).

For the Nano-Enabled I^3. The anionic polymer-drug solution (0.3 mL) was distributed to plastic moulds (diameter = 12 mm, volume = 1 cm^3, curvature = 10°) containing 0.05 mL of an acidified 3%$^{w}/_{v}$ $AlCl_3$ solution, where the $AlCl_3$ serves as a catalyst for the interpolymeric coupling reaction (Friedel-Crafts acylation). The cationic polymer solution (0.1 mL) was added to the center of the mould. Diffusional development of two separate interpenetrating networks, and simultaneous curing of the chitosan core (inner BPM) and outer BPM, was allowed to occur over 12 h. The final implants were washed thrice with double deionized water and allowed to dry for 48 h under ambient conditions at 25°C.

Molecular Modeling Simulations for Prediction of Pertinent Interactions between the I^3 and Normal or Inflammatory Ocular Milieu

The concept of computational chemistry and molecular modeling relates to the application of theoretical methods and computational techniques for the modeling and simulation of small chemical and biological systems in order to predict and interpret their behavior, and is significantly applicable to polymeric systems implicated in the formation of a novel drug delivery system as exemplified, in this investigation, by the I^3. All modeling procedures, computations, and molecular simulations were performed using commercial softwares: HyperChem™ 8.0.8 Molecular Modeling System (Hypercube Inc., Gainesville, Florida, USA) and ChemBio3D Ultra 11.0 (CambridgeSoft Corporation, Cambridge, UK). Simulation approaches included molecular mechanics (MM) and molecular dynamics with the number of atoms, pressure and temperature held constant (NPT-MD).

Static Lattice Atomistic Simulations in a Solvated System

The decamer of polyacrylic acid (PAA) was archetyped using ChemBio3D Ultra in its syndiotactic stereochemistry as a 3D model, whereas the structures of alginate (ALG; 6 monosaccharide units) and hyaluronic acid (HA; 6 monosaccharide units) was built from standard bond lengths and angles using the Sugar Builder Module on HyperChem 8.0.8. To generate the final models in a solvated system, the MM simulations were performed for cubic periodic boxes with the polymer/polymer at the center of the cubic box and the remaining free space filled with water molecules and primarily energy-minimized using the MM + Force Field algorithm and the resulting structures were subsequently energy-minimized using the AMBER 3 (Assisted Model Building and Energy

Refinements) Force Field algorithm. The force fields were utilized with a distance-independent dielectric constant with no scaling (Table I). Additionally, the Force field options in the AMBER (with explicit solvent) were extended to incorporate cutoffs to inner and outer options with the nearest-image periodic boundary conditions, and the outer and inner cutoffs were to ensure that there were no discontinuities in the potential surface (19).

Molecular Mechanics Assisted Model Building and Energy Refinements

A molecular mechanics conformational searching procedure was employed to acquire the data required in the statistical mechanics analysis, to obtain differential binding energies of a Polak-Ribiere algorithm, and to potentially permit application to polymer composite assemblies. MM + is a HyperChem modification and extension of Norman Allinger's Molecular Mechanics program MM2 (20) whereas AMBER is a package of computer programs for applying molecular mechanics, normal mode analysis, molecular dynamics and free energy calculations to simulate the structural and energetic properties of molecules (21).

Molecular mechanics energy relationship (MMER), a method for analytico-mathematical representation of potential energy surfaces, was used to provide information about the contributions of valence terms, noncovalent Coulombic terms, and noncovalent van der Waals interactions for polymer/ polymer interactions. The MMER model for the potential energy factor in various molecular complexes can be written as:

$$E_{molecule/complex} = V_{\Sigma} = V_b + V_\theta + V_\varphi + V_{ij} + V_{hb} + V_{el} \quad (1)$$

Where V_{Σ} is related to total steric energy for an optimized structure, V_b corresponds to bond stretching contributions (reference values were assigned to all of the structure's bond lengths), V_θ denotes bond angle contributions (reference values were assigned to all of the structure's bond angles), V_φ represents torsional contribution arising from deviations from optimum dihedral angles, V_{ij} incorporates van der Waals interactions due to non-bonded interatomic distances, V_{hb} symbolizes hydrogen-bond energy function, and V_{el} denotes electrostatic energy.

In addition, the total potential energy deviation, ΔE_{total}, was calculated as the difference between the total potential energy of the complex system and the sum of the potential energies of isolated individual molecules, as follows:

$$\Delta E_{Total(A/B)} = E_{Total(A/B)} - \left(E_{Total(A)} + E_{Total(B)}\right) \quad (2)$$

The molecular stability can then be estimated by comparing the total potential energies of the isolated *versus* the complexed systems. If the total potential energy of the complex is smaller than the sum of the potential energies of isolated individual molecules in the same conformation, the complexed form is more stable and its formation is favored (22).

Table I Computational Parameters Used to Construct Aqueous-Phase Model Building and Simulations

S. No.	Parameter	Description
1	Periodic box dimensions	$15 \times 15 \times 20 A^{\circ 3}$
2	Cut-offs	Switched
3	Dielectric (epsilon)	Constant
4	1–4 Scale factors	Electrostatic: 0.5 van der Waals: 0.5
5	Outer radius	7.5A°
6	Inner radius	3.5A°
7	Water molecules	149
8	Solvent/Polymer distance	2.3A°

Rheological Analysis of the Initiator Polymer-Crosslinker Milieu for Determination of the Physicomechanical Expression of the Stimulus-Responsive Behavior

Oscillatory studies are of importance for the evaluation of the multipolymeric hydrogels (referred to as stimulus-responsive hydrogel systems, SRHS) forming the matrices to be exposed to crosslinking agents, as they are anticipated to undergo macro- or micro-structural rearrangement with time. These rearrangements directly influence rheological performance, which in turn could provide the necessary information regarding 'stimulus-responsive' transitions in the polymeric components of the I^3 with time (23).

Preparation of the Precursor Stimulus-Responsive Hydrogel Systems

For the SRHS forming the intermediate release BPM, a $4\%^{w}/_{v}$ sodium alginate-$1\%\ ^{w}/_{v}$ PAA (Carbopol 974)-$3\%^{w}/_{v}$ NHS-$0.25\%^{w}/_{v}$ HA-$2.5\%^{v}/_{v}$ gluteraldehyde-$0.25\%^{w}/_{v}$ ciprofloxacin aqueous solution was prepared, instituting carbodiimide coupling chemistry to increase the interconnectivity of the matrix. DCC (300 mg) was dissolved in ethanol and dispersed within the polymeric solution. This solution constituted the outer BPM SRHS (A). Incremental amounts of the cationic chitosan SRHS (inner BPM) incorporating the Lipo-CHT-PCL NS (B) was added to the anionic SRHS, and the rheological transitions ascertained. Additionally incremental concentrations of an acidified $3\%^{w}/_{v}$ $AlCl_3$ solution (C) was added to the anionic polymeric composition of certain samples, thus serving as the initiator solution.

Oscillatory Studies: Frequency Sweep Tests

The oscillatory studies of the sample hydrogel systems were carried out employing the Thermo Scientific HAAKE MARS Rheometer (Thermo Fischer Scientific, Karlsuhe, Germany). The frequency sweep tests were carried out at the frequency range of 0.05-1Hz at a temperature of 37°C. Two sample gel systems were tested, as per the preferred ratio of components identified during preliminary analysis:

(i) The outer and inner BPM SRHS (A:B) (1 mL: 0.5 mL)
(ii) The system comprising of all three BPM components: the outer BPM SRHS, the inner BPM SRHS, and the initiator solution (A:B:C) in a ratio of 1 mL: 0.5 mL: 0.1 mL, respectively.

These two systems (i and ii) in their respective concentrations were used to perform the frequency tests in response to simulated ocular inflammatory conditions and normal ocular conditions. Frequency sweep tests were carried out after exposing a set of each of the solutions to normal conditions in 4 mL normal simulated vitreous humor (SVH, comprising phosphate-buffered saline with 0.03%$^{v}/_{v}$ HA, 37°C,pH 7.4) and another set to inflammatory conditions in 4 mL SVH containing 0.05 M Fenton's reagent (which generated 100 μmol of hydroxyl radicals following combining $FeSO_4$ and 0.1 M H_2O_2) for a period of 28 days, simulating normal ocular physiological conditions and ocular inflammatory conditions, respectively. The frequency sweep tests were time dependent, carried out on days 0, 3, 7, 14, 21 and 28. A second set of frequency sweep analyses was performed by alternating the two solutions between normal SVH and Fenton's Reagent in SVH in the same above mentioned conditions. Dialysis tubing cellulose membrane (flat width: 33 mm, diameter: 22 mm, MW: 12400, Sigma-Aldrich®, St. Louis, MO, USA) was used to encase and expose the respective systems to normal SVH and Fenton's Reagent in SVH. All investigations were conducted in triplicate ($n = 3$).

Characterization of Vibrational Transitions by Fourier Transform Infrared Spectroscopy

Fourier Transform Infrared Spectroscopy (FTIR) was applied to the study of the I^3, for system exemplification and investigation of its structured properties e.g. crystallinity and hydrogen bonding. The vibrational molecular transitions of the outer and inner matrix (comprising the NS incorporated within a crosslinked chitosan core) in comparison with the native system components were characterized for the attainment of important microstructural information via their FTIR spectra, recorded on a PerkinElmer® Spectrum 100 Series fitted with a universal ATR Polarization Accessory (PerkinElmer Ltd., Beaconsfield, UK). Spectra were recorded over the range 4,000–625 cm^{-1}, with a resolution of 4 cm^{-1} and 32 accumulations.

Characterization of Thermal Transitions of the I^3 by Advanced Differential Scanning Calorimetry

Knowledge of the glass transition (T_g) is vital in the enhancement of the novel drug delivery device. It is reported that the modification in T_g of a polymer is dependent on the interaction degree between the componential polymers and the polymers and drug. An increase in the temperature is substantially associated with a strong interaction, which is essentially dictated by a fall in the polymer chain mobility—the nature of the chemical crosslinking interactions are inherent to defining the success of the proposed implant (24).

Because crosslinking increases the T_g of a polymer following the introduction of molecular restrictions, Nielson (25) averaged the data in the literature to arrive at the following empirical equation:

$$T_g - T_{g0} = \left(3.9 \times 10^4\right)/M_c \tag{3}$$

M_c is the average molecular weight between crosslinked points, to be considered with reference to the M_w of the native polymer. T_{g0} is the T_g of the uncrosslinked polymer having the same chemical composition as the crosslinked polymer.

Assessment of the thermal transitions was performed on all native polymers and drugs and compared with the formed inner and outer BPMs employing a Temperature Modulated Differential Scanning Calorimeter (TMDSC) (Mettler Toledo DSC-1 STAR^e System, Schwerzenback, ZH, Switzerland). Normal and temperature-modulated DSC curves were generated. Thermal events of significance included the glass transition (T_g), measured as the reversible heat flow due to changes in the magnitude of the C_p-complex values (ΔC_p); and melting (T_m) and crystallization (T_c) temperature peaks which are consequences of irreversible heat flow corresponding to the total heat flow. The temperature calibration was undertaken in accordance with the melting transition of indium. Samples were weighed on perforated 40 μL aluminium pans and evaluated over the temperature range of interest under nitrogen atmosphere (Afrox, Germiston, Gauteng, South Africa) in order to diminish oxidation. The instrument parameters are highlighted in Table II.

On-Off Inflammation-Responsive *In Vitro* Drug Release Capabilities of the I^3

Intrinsic to the *modus operandi* of the I^3 was its *in vitro* drug release performance with interchanging exposure to *and* removal of the mitigating (inflammatory) stimulus. A modified closed-compartment USP 31 dissolution testing apparatus was used. Each accurately weighed I^3 (for this study, separately loaded with either indomethacin in the core BPM or ciprofloxacin in the outer BPM) was alternated between normal conditions (N) following immersion in 4 mL normal SVH at physiological pH

Table II TMDSC Settings for Thermal Analysis

Segment Type	Parameter Setting
SINE[a]	
Start	0°C
Heating rate	1°C/min
Amplitude	0.8°C
Period	0.8°C
LOOP[b]	
To segment	1
Increment	0.8°C
End	≥200°C (varies with the polymer)

[a] Sinusoidal Oscillations

[b] Oscillation periods

(7.4), or pathological inflammatory conditions (F) in 4 mL SVH containing 0.05 M Fenton's reagent (which generated 100 μmol of hydroxyl radicals). This level of hydroxyl radicals fell within the range of hydroxyl radicals reportedly generated during pathological inflammatory states (26). The I^3 was thus exposed to alternating normal and inflammatory phases as highlighted in Table III.

The samples were placed in closed vials and placed in an oscillating laboratory incubator (Labcon® FSIE-SPO 8–35, California, USA), set to 20 rpm. At 3, 7, 14, 21 and 28 days, the respective media was subjected to UV spectrophotometric analysis before being drained and replaced with new media. All aliquots withdrawn were subjected to filtration (0.22 μm PVDF, Millipore Corporation, Bedford, MA, USA) and appropriately diluted prior to spectrophotometric analysis (Specord 40 UV spectrophotometer, Analytik Jena AG, Jena, Germany) at the λ_{max} for indomethacin (318 nm) and ciprofloxacin (278 nm) in SVH (Note: the UV methodology was evaluated for linearity, accuracy, precision, reproducibility, and specificity). The componential polymeric absorbance of the I^3, together with the influence of the Fenton's reagent on the absorbance readings at the respective wavelengths were taken into account. All analyses were conducted in triplicate ($n=3$).

Table III Exposure Conditions for Assessment of the On-Off Inflammation-Responsive Capabilities of the Optimum Formulation

Time period	Condition	Media
Day 0–3	Normal	SVH
Day 3–7	Inflammatory	SVH + Fenton's reagent
Day 7–14	Normal	SVH
Day 14–21	Inflammatory	SVH + Fenton's reagent
Day 21–28	Normal	SVH

Magnetic Resonance Imaging for Live-Acquisition of the Inflammation-Responsive Transitions of the I^3

Magnetic Resonance Imaging (MRI) has specific application for its potential to monitor the fate of the dosage form *in vivo*, and attractively, to correlate *in vitro* with *in vivo* behavior. For complex systems comprised of a number of functional polymeric excipients, thorough comprehension of the drug release mechanism is difficult employing cumulative drug release profiles alone. The kinetics of water ingress into the drug delivery system has a significant contribution in controlling drug release from hydrogel matrices (27). Application of MRI to the long-term hydrational behavior of a complex polymeric system is a largely unexplored aspect. This investigation sought to gain further insight into the extent of water ingress into the I^3 over a prolonged period, as well as ascertaining the opposing intricacies of water uptake under normal *versus* pathological conditions. MRI was thus used in this study to probe the movement of water within the I^3 on exposure to and removal of the inflammatory stimulus.

A magnetic resonance system with digital MARAN-i System configured with a DRX2 HF Spectrometer console (Oxford Instruments Magnetic Resonance, Oxon, UK) equipped with a compact 0.5 Tesla permanent magnet stabilized at 37°C and a dissolution flow through cell was employed for the viewing of the hydrational morphological transitions of the I^3. Following configuration, shim optimization and probe tuning, the cone-like lower part of the cell was filled with glass beads to provide laminar flow at 16 mL/min of the solvents employed. The implant matrices were placed in position each time following dissolution analysis (described below) within the cell which in turn was positioned in a magnetic bore of the system and MR images were acquired every 3 min with MARAN-i version 1.0 software. Image acquisition was achieved following setting of the frequency offset and testing gain employing RINMR version 5.7 under continuous solvent flow conditions. MARAN-i software comprises image acquisition software and image analysis software. The image acquisition parameters are depicted in Table IV.

The I^3 was exposed to SVH and another to SVH and Fenton's Reagent for a period of 28 days ($n=3$). The MR images were taken on days 0, 3, 7, 14, 21 and 28 in order to visually determine implant hydration. In a further investigation, the I^3 was alternated between SVH and Fenton's reagent at days 0, 3, 7, 14, 21 and 28; following exposure to conditions as described in the *in vitro* drug release study above (Table III). Image acquisition was performed in triplicate at each time point ($n=3$). The gelled intensity and change in area of the I^3 was ascertained for each time point.

MRI was undertaken concurrently with *in vitro* drug release evaluations in an effort to correlate the drug release behavior with the observed changes in the implant appearance and hydration state on exposure to and removal of the inflammatory

Table IV Image Acquisition Parameters Applied During Magnetic Resonance Imaging Employing the MARAN-i

S. No.	Parameter	Value
1.	Imaging protocol	FSHEF
2.	Requested gain (%)	4.17
3.	Signal strength	68.92
4.	Average	2
5.	Matrix size	128
6.	Repetition time (ms)	1000.00
7.	Spin Echo Tau (ms)	6.80
8.	Image acquired after	60 min
9.	Total scans	64

stimulus. Thus, analysis of all corresponding dissolution samples via UV spectroscopy was performed, as described ($n = 3$).

Morphological Characterization and Image Processing Analysis of Erosional Behavior of the I^3

In order to describe the inflammation-responsive morphological transitions of the device, the I^3 was exposed to normal and inflammatory conditions over 28, 56 and 72 days and transitions in surface architecture visualized via scanning electron microscopy (SEM). The implants were coated using the SPL module-Sputter Coater (Toronto, Canada). The sample implants were attached to the spud using carbon paper and were left in the SPL module-Sputter Coater for 120 s to ensure generously coated surfaces. The SEM images were taken with the objective of comparing surface changes related to the bioerosion mechanism of the device when exposed to normal *versus* inflammatory conditions, using the Phenom G2 Pro SEM (Germany).

To enhance characterization of the microscopic images, image analysis was undertaken employing intricate mathematical software (Mathematica® v. 8.0, Wolfram Research Inc., Champaign, IL, USA) in accordance with an approach previously developed (28). For the erosional images acquired via SEM, image processing was performed on sixteen-bit greyscale images obtained by SEM of the inner and outer BPMs of the I^3. These images were low in contrast due to the effects of uneven illumination across the field of view. Thresholding of crude images was unable to capture all of the required details; therefore intermediate image-processing steps were employed to even out the background and increase contrast between the solid polymeric architecture, deep pores, and pores at the surface of the structure. Images in TIFF format were imported and converted to Mathematica™ 8.0 format.

The first processing step, blurring the image, provided a distorted version of the image making it unfocused, which can be obtained by convolving the image with a low pass filter. For this investigation, the quantity of blurring is increased by increasing the pixel radius (r) to 15 without compromising image detail. This was achieved in Mathematica™ 8.0 by applying a custom blurring function (Eq. 4, where *'Image'* refers to the applicable SEM image file):

$$Blur[\text{'}Image\text{'}, 15] \tag{4}$$

After blurring the image, the next step was to ColorQuantize the blurred image at 5 which provided an approximation to an image that uses only 5 distinct colors. This was achieved in Mathematica™ 8.0 by applying a custom ColorQuantize function:

$$ColorQuantize[\text{'}Image\text{'}, 5] \tag{5}$$

The third step consisted of analyzing the images by plotting a histogram. Histograms of both the unmodified SEM and well as the color quantized image were plotted in order to exemplify the extent of refinement provided by the image manipulation, for assisting description of the overall implant architecture. This default function plots a histogram of the pixel levels for each channel in the image, which was represented as 'voxel intensity', where a voxel is a 'volumetric pixel', carrying the same color-intensity properties as pixels, plus the additional important property of transparency. Furthermore, separate histograms for each color channel were constructed. This was achieved in Mathematica™ 8.0 by applying the custom ImageHistogram functions for default and separated algorithms as displayed in Eq. 6:

$$ImageHistogram[\text{'}Image\text{'}, Appearance \rightarrow \text{"}Transparent\text{"}] \tag{6}$$

An analysis of the histogram was essential for the best choice of the threshold for discriminating between different morphological features seen in the SEM of the eroding I^3.

In Vivo Analysis of the Inflammation-Responsive Behavior of the I^3 in the Rabbit Eye

Ethics clearance for the ensuing *in vivo* investigation was obtained from the Animal ethics Committee of the University of the Witwatersrand, Ethics Clearance No. 2009/02/05.

In Vivo Design and Surgical Technique in the Healthy Rabbit Eye

In order to obtain preliminary 7 day ocular levels of both indomethacin and ciprofloxacin, ten New Zealand Albino rabbits (free of any signs of ocular inflammation or gross

abnormality) were used, randomly assigned to the experimental (5 rabbits) and control (5 rabbits) groups. A placebo (drug-free) device was implanted into one eye of the control group and the drug-loaded implant into one eye of the experimental group. The minimum animal sample size for testing was ascertained from the specifications of the Animal ethics Committee of the University of the Witwatersrand for statistical significance (i.e. $n=5$ for each sample point).

All procedures were in accordance with the Association for Research in Vision and Ophthalmology (ARVO) Statement for the Use of Animals in Ophthalmic and Vision Research. Animals were housed at room temperature with a 12-h light/dark cycle (light from 6 am to 6 pm), and were fed a standard rabbit diet with water available *ad libitum*. Following induction of general anesthesia via intramuscular administration of ketamine HCl, 40 mg/kg (a dissociative anesthetic) and xylazine HCl, 10 mg/kg (a sedative, anesthetic, muscle relaxant, and analgesic) and local anesthesia via instillation of tetracaine HCl 0.5%$^{w}/_{w}$ (topical anaesthetic), the operative eye was prepared in a sterile manner and a wire lid speculum inserted. Sub-Tenon implantation was preferentially identified for device placement following pilot studies. A small peritomy was created supero-temporally and a tunnel made into the sub-Tenon space extending as far posterior as possible. The device was grasped with a blunt forceps and pushed into the sub-Tenon pocket such that the anterior edge of the device was at least 10 mm back from the limbus. The device was left between superior and lateral rectus muscles and no additional securing was required. The conjunctiva and Tenon's capsule were pulled over to cover the device completely and secured at the limbus with a single 9–0 Nylon suture with the knot buried. Chloramphenicol ointment 1%$^{w}/_{w}$ was instilled into each eye after surgery for the prevention of surface ocular infections of the conjunctiva and/ or cornea. Recovery and post-surgical care was initiated and visual assessment was conducted daily with the rabbits observed for any untoward changes (e.g. retinal detachment and intravitreal hemorrhage) which would warrant termination of the study.

On day 7, all animals were euthanized with an overdose of IV sodium pentobarbitone (>50 mg/kg, ~2 mL) at each sampling point with consequent enucleation. The central vitreous humor (approximately 2 mL) from the enucleated eye was aspirated employing a 15″ needle (hyalocentesis). Therefter, the adherent muscle tissue was removed from the eye and the anterior segment of the eye was removed with a circumferential cut behind the limbus. The remaining orbital tissues were stored with the vitreous samples to enable measurement of drug (not yet internalized for intracellular mechanisms) in the choroid (posterior component of uvea), and retinal pigment epithelium (RPE) tissues. The tissues and vitreous were immediately snap-frozen at −80°C in an ultra-low freezer (Sanyo VIP™ Series, Sanyo North America Corporation, Wood Dale, IL, USA).

In Vivo Design and Surgical Technique in the Inflamed Rabbit Eye

In order to detect the inflammation-responsive behavior of the I^3 *in vivo*, drug release investigations were pursued in the inflamed rabbit eye. Intraocular injection of lipopolysaccharide (LPS) for induction of ocular inflammation as an acute endotoxin-induced uveitis (EIU) in the right eye of the rabbit was thus performed (29), i.e. one eye was exposed to the inflammatory stimulus. Ten New Zealand Albino rabbits were used, assigned to experimental (5 rabbits) and control (5 rabbits) ($n=5$ at the sampling point on day 7). Device implantation in the control and experimental groups was on day 0, as described for the normal rabbit eye. On day 3, intraocular inflammation was induced via intravitreal injection (100 μL) of *Salmonella typhimurium* LPS (100–200 ng/10 μL of phosphate-buffered saline) into one eye. The diluted LPS was injected intravitreally at the pars plana 2.0 mm posterior to the limbus using a needle, taking care to avoid injury to the lens, following general anesthesia as described. All rabbits were euthanized on day 7 with sodium pentobarbitone, the implant removed, and the central vitreous humor (≈2 mL) from the enucleated eye was aspirated with a needle, and the ocular tissues stored as described for the normal rabbit eye. The results of the investigations from both normal and inflamed groups would allow ascertainment of the purported differences in drug release behavior in the healthy *versus* the inflamed rabbit eye for ultimate description of the clinical potential of the I^3.

Determination of the Erosional Behavior of the I^3 in the Normal and Inflamed Rabbit Eye

The dynamic weight change of the drug-loaded device before implantation and following removal from the euthanized rabbit at 7 days was assessed in the normal and inflamed rabbit eye. Following removal of the I^3 from the eye, it was allowed to dry under normal conditions to constant weight. The following empirical relationship was used to demonstrate the overall gravimetric transition of the I^3 from 100% to 0% initial weight:

$$I^3 erosion(\%) = \left(\frac{initial\ weight - final\ weight}{initial\ weight}\right) \times 100 \qquad (7)$$

The initial and final weights represent the pre-implantation and dried post-implantation weights of the I^3, respectively. Measurements were undertaken in quintuplicate ($n=5$).

Quantification of In Vivo Anti-Inflammatory and Antibiotic Concentrations Released from the I^3 into the Posterior Segment of the Rabbit Eye Model under Normal and Inflammatory Conditions

A method was required for simultaneous detection of ciprofloxacin and indomethacin in rabbit posterior ocular fluid. An

ultraperformance liquid chromatographic (UPLC) method was developed employing a Waters® ACQUITY™LC system (Waters®, Milford, MA, USA) coupled with a photodiode array detector (PDA), and Empower® Pro Software (Waters®, Milford, MA, USA). The UPLC was fitted with an Aquity UPLC® Bridged ethyl Hybrid (BEH) Shield RP_{18} column, with a pore size of 1.7 μm. A gradient method with a run time of 4 min was developed using acetonitrile and 0.1%$^{v}/_{v}$ formic acid in double deionized water as the mobile phase (Table V). UPLC analysis reveals new information about the samples under investigation and reduces the risk of non-detection of potentially important co-eluting analytes.

A solvent flow rate of 0.25 mL/min was maintained with an average initial pressure of 6,500 psi. The extracted and pre-filtered samples (0.2–1.0 μL) were injected onto the column. The column and sample manager temperature was maintained at 21 ± 0.5°C. Prior to use, the column was equilibrated by passing 45 mL of mobile phase solvent through the system. The eluent was monitored at analytical wavelengths set at 254, 278 and 318 nm and the entire assay procedure was performed at room temperature (21 ± 0.5°C).

Nicotinic acid was identified via preliminary screening assays as an appropriate internal standard for both indomethacin and ciprofloxacin, being separated employing the mobile phase system instituted, and possessing an isolated retention time for sound analysis of peak areas. A standard linear curve was generated, as subsequently described to assess the respective drug concentrations released from the device at various time points.

Preparation of Calibration Standards

In order to prepare the blank rabbit vitreous humor-posterior segment tissue dissolutes sample, a sample eye in which a no I^3 was implanted was employed. Rather than homogenize the posterior segment tissues together with the vitreous (as has been previously undertaken in certain investigations such as those of Cheruvu *et al*. (30)) the posterior segment tissues (inclusive of choroid and RPE) together with the associated 2 mL vitreous were prepared as follows to extract the drugs: the stored and frozen blank samples were thawed at room temperature (21 ± 0.5°C) and allowed to environmentally equilibrate, followed by centrifugation at 15,000 × *g* for 10 min. Centrifugation was repeated twice in order to release any drug present in the tissues (which would be absent in the unimplanted eye). The supernatant was isolated and henceforth referred to as the total posterior ocular fluid (TPOF). Stock solutions of indomethacin and ciprofloxacin were prepared (0.2 mg/mL) and diluted further with deionized water to prepare spiking solutions with indomethacin and ciprofloxacin concentrations ranging between 0.02 and 0.1 mg/mL. To prepare the calibration standards used for generating a standard curve of indomethacin and ciprofloxacin in TPOF and for method validation, 50 μL aliquots of both indomethacin and ciprofloxacin spiking solutions and the internal standard solution of nicotinic acid (100 μL; initial concentration of 0.2 mg/mL) were added to inert polypropylene tubes, each tube contained a 200 μL aliquot of blank rabbit TPOF previously thawed and centrifuged at 15,000 × *g* for 10 min. A liquid-liquid phase extraction methodology was used for the extraction of all drugs added from the blank rabbit TPOF to prepare a calibration profile. To each calibration standard, 300 μL of acetonitrile was added. The tubes were then capped, vortexed (Vortex-Genie 2; Scientific Industries Inc., Bohemia, New York) for 15 s and centrifuged (Optima R LE- 80 K, Beckman Coulter Inc., Fullerton, California) at 15,000 × *g* for 10 min. Aliquots (300 μL) of the supernatants were filtered through a 0.22 μm Millipore® filter and transferred to UPLC injection vials. Thereafter, 0.2 μL of the filtered solution was injected onto the UPLC column for simultaneous indomethacin and ciprofloxacin content analysis. The ratio of the peak areas (between the internal standard nicotinic acid, and indomethacin and ciprofloxacin) *versus* the concentration data for the calibration standards was fit by linear regression to generate the calibration curves. This procedure generated a set of five calibration standards with concentrations ranging from 0.109645 to 0.520813 μg/mL of indomethacin/ ciprofloxacin in rabbit TPOF. The five calibration standards were used to construct a standard linear curve and additional calibration standards were prepared and analyzed for validation runs for precision and accuracy analysis of the assay method ($n = 3$). Accuracy was assessed by evaluation of mean recovery, defined as the ratio of mean found concentration to nominal concentration, expressed as a percentage. Recovery of both drugs during the extraction procedures in the TPOF samples was thus assessed by replicate analysis ($n = 3$) of the lower and upper concentration limits of the calibration standards and compared to those obtained by injection of aqueous solutions of indomethacin and ciprofloxacin prepared at the same concentrations corresponding to the standards. Both extracted calibration standards and the aqueous samples were injected onto the UPLC column employing the same chromatographic conditions as in the assay method developed.

Table V Gradient Method for the Separation of Indomethacin and Ciprofloxacin Indicating Mobile Phase Concentrations at Flow Rates at Each Time Point Over the 3 Min Run Time

Time (min)	Flow rate (mL/min)	0.1%$^{v}/_{v}$ Formic acid solution	Acetonitrile
Initial	0.5	85	15
1.00	0.5	20	80
3.00	0.5	85	15

Extraction of Indomethacin and Ciprofloxacin from the Aspirated Vitreous Fluid and Posterior Segment Tissue Samples

The stored and frozen study samples were thawed at room temperature (21 ± 0.5°C) and allowed to environmentally

equilibrate, followed by centrifugation at 15,000×*g* for 10 min. Centrifugation was repeated twice in order to release any drug present in the tissues. The supernatant was isolated, representing the TPOF and total drug. The sample biological matrix was replicated in the matrix employed for the calibration standards. Aliquots (200 μL) of the TPOF samples were transferred using a graded microsyringe (0.5 μL) [Hamilton (Pty) Ltd., Bonaduz, GR, Switzerland] into polypropylene tubes. The internal standard in deionized water (nicotinic acid; 0.2 mg/mL; 100 μL) was added to each tube, and the tubes were vortexed for 15 s. The same procedure used for the extraction of the calibration standards (with the addition of 300 μL acetonitrile), and UPLC injection of calibration standards, were applied to the diluted TPOF samples for simultaneous measurement of indomethacin and ciprofloxacin content. Measurements were conducted in triplicate ($n=3$).

Histomorphological Analysis for Assessment of the Degree of Ocular Inflammation Following Implantation of the I^3 in the Normal and Inflamed Rabbit Eye

Concurrently with drug release studies, an additional group of rabbits were exposed to the same surgical procedures as described for the *in vivo* implantation studies, depending on their assigned group, with euthanasia and enucleation at day 7, but no collection of TPOF samples. Rabbits were assigned to the following groups ($n=3$ for each group):

- Control (no inflammation induction and no I^3 implantation)
- LPS Injection (no I^3 implantation)
- Drug-free I^3—normal eye
- Drug-loaded I^3—normal eye
- Drug-free I^3—inflamed eye
- Drug-loaded I^3—inflamed eye

The enucleated eyeballs (fixed in $10\%^{v}/_{v}$ formalin) were sent to IDEXX laboratories (Pretoria, South Africa) and were sectioned along the sagittal axis close to the optic nerve at three different levels. The sections were processed overnight in an automated tissue processor according to their standard operating procedure (PTA-his-SOP-27). Following the routine histological processing, wax blocks were produced in paraffin wax and sections of approximately 6 μm cut according to IDEXX SOPs (PTA-his-SOP-30). The slides were stained with hematoxylin and eosin according to the IDEXX SOPs (PTA-his-SOP-49).

Cellular infiltration (degree of infiltration by lymphocytes, plasma cells, and mononuclear and polymorphonuclear leukocytes) was graded from 0 to 3+ in accordance with IDEXX laboratory protocols, as instituted in related investigations (31).

RESULTS

Molecular Modeling Simulations for Prediction of Pertinent Interactions between the I^3 and Normal or Inflammatory Ocular Milieu

The polymeric system comprising the outer BPM (modeled as bi- and tripolymeric complexes) were modeled in the presence of a solvated system with water as the solvent at room temperature. The dimensions of the periodic box were maintained and hence the number of water molecules per molecular system was constant. The final optimized solvated architectures for the bipolymeric architectures were destabilized as compared to the monopolymeric (individual) molecules under similar conditions (Eqs. 8–13). The final optimized static energy for the tripolymeric ALG-PAA-HA-H_2O was much lower than either of the individual polymers: ALG-H_2O; PAA-H_2O; or HA-H_2O (Eqs. 8, 9, 10 and 14) and the bipolymeric molecular complexes: ALG-PAA-H_2O; PAA-HA-H_2O; or PAA-HA-H_2O (Eqs. 11–14) (Fig. 1a).

$$E_{ALG-H2O} = -4182.155V_{\sum} = 47.936V_b + 73.647V_\theta + 51.075V_\varphi + 82.174V_{ij} - 16.299V_{hb} - 4420.69V_{el} \quad (8)$$

$$E_{HA-H2O} = -4154.776V_{\sum} = 49.986V_b + 84.461V_\theta + 79.982V_\varphi + 88.341V_{ij} - 14.607V_{hb} - 4442.94V_{el} \quad (9)$$

$$E_{PAA-H2O} = -3705.359V_{\sum} = 38.304V_b + 43.612V_\theta + 8.100V_\varphi + 78.321V_{ij} - 4.155V_{hb} - 3869.54V_{el} \quad (10)$$

$$E_{ALG-PAA-H2O} = -3826.993V_{\sum} = 43.983V_b + 73.445V_\theta + 74.001V_\varphi + 88.212V_{ij} - 33.950V_{hb} - 4072.68V_{el} \quad (11)$$

$$E_{ALG-HA-H2O} = -3882.668V_{\sum} = 49.303V_b + 121.86V_\theta + 104.302V_\varphi + 81.720V_{ij} - 40.815V_{hb} - 4199.04V_{el} \quad (12)$$

$$E_{PAA-HA-H2O} = -3675.562V_{\sum} = 41.485V_b + 75.155V_\theta + 60.084V_\varphi + 60.355V_{ij} - 26.229V_{hb} - 3886.41V_{el} \quad (13)$$

$$E_{ALG-PAA-HA-H2O} = -4592.788V_{\sum} = 59.645V_b + 134.86V_\theta + 150.876V_\varphi + 96.631V_{ij} - 49.856V_{hb} - 4984.94V_{el} \quad (14)$$

This substantial decrease in energy values for the tripolymeric structure is evidenced by all the non-bonding

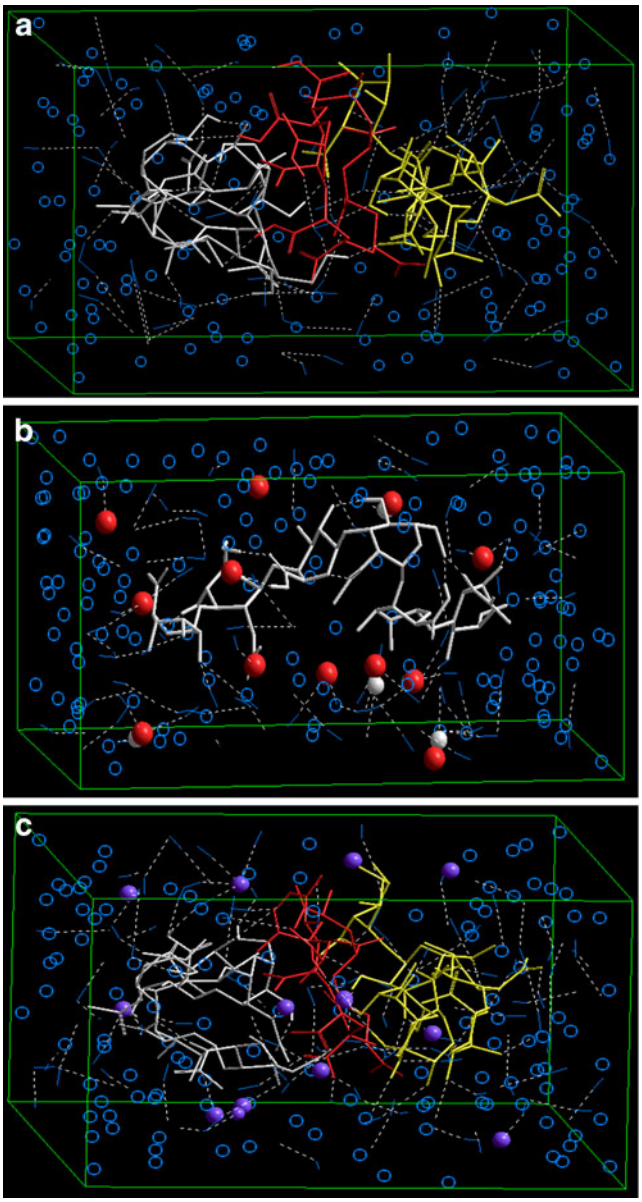

Fig. 1 (**a**) Visualization of the geometrical preference of the tripolymeric complex consisting of alginate (*yellow*), polyacrylic acid (*red*), and hyaluronic acid (*white*) after molecular simulation in a solvated system consisting of water molecules (*blue molecules*). (**b**) Visualization of geometrical preference of hyaluronic acid (*white tubes*) and hydroxyl ions (*red balls*). (**c**) Visualization of geometrical preference of tripolymeric complex consisting of alginate (*yellow*), polyacrylic acid (*red*), and hyaluronic acid (*white*) in response to addition of hydroxyl ions (*purple balls*) after molecular simulation in a solvated system consisting of water molecules (*blue molecules*).

energy contributing towards the structural stabilization, with enhanced H-bonding and electrostatic interactions. This supports the institution of the tripolymeric system for forming a well-complexed outer BPM.

The OH^--mediated stimuli-responsive behavior of the outer BPM is presented in Fig. 1b and c. The MMER analysis confirmed the interaction potential of the OH^- with polysaccharides accounting for stabilized binding energies of −3383.307 kcal/mol (Eqs. 9 and 15) and −2541.329 kcal/mol (Eqs. 14 and 16) for HA and ALG-PAA-HA molecular complexes, respectively.

$$E_{HA-H2O-OH} = -7538.083V_{\Sigma} = 86.210V_b + 125.944V_{\theta} + 85.995V_{\varphi} + 207.547V_{ij} - 12.752V_{hb} - 8031.03V_{el} \quad (15)$$

$$E_{ALG-PAA-HA-H2O-OH} = -7044.117V_{\Sigma} = 96.147V_b + 215.22V_{\theta} + 157.456V_{\varphi} + 290.264V_{ij} - 52.878V_{hb} - 7750.33V_{el} \quad (16)$$

Oscillatory Studies: Frequency Sweep Tests

Oscillatory studies were undertaken for characterization of the effect of macro- and micro-structural rearrangements on rheological performance with the initiation of crosslinking within the inner and outer SRHS forming the I^3, and on their exposure to and following the removal of the inflammatory stimulus. The SRHS for the outer and inner BPM are represented by A and B, respectively, whereas C represents the initiator solution of $AlCl_3$. Results are reported in terms of the average loss tangent (Fig. 2), where the loss tangent is the tangent of the phase angle—the ratio of viscous modulus to elastic modulus and a useful quantifier of the presence and extent of elasticity in a fluid, as per Eq. 17. With a $\tan\delta$ value of 1, the elastic (solid-like) and viscous (liquid-like) properties of the material are equal. The smaller the loss tangent is, the more elastic the material. *Tan* δ is often the most sensitive indicator of various molecular motions within the material. In general, the smaller the $\tan\delta$ (or the greater G'), the stronger is the interaction.

$$\tan\delta = G''/G' \quad (17)$$

Figure 2a depicts that both A:B and A:B:C displayed a progressive increase in the loss tangent, with the loss tangent exceeding 1 after only 3 days for A:B:C, thus liquid-like characteristics were observed and prevailed for the precursor BPM solutions, specifically where crosslinking was initiated, when exposed to inflammatory conditions.

Both A:B and A:B:C exhibited stimulus-responsive rheological behavior on exposure to and removal of the inflammatory environment. The average loss tangent was highest when exposed to Fenton's reagent on day 7, specifically for A:B:C, with liquid-like characteristics predominating (Fig. 2b).

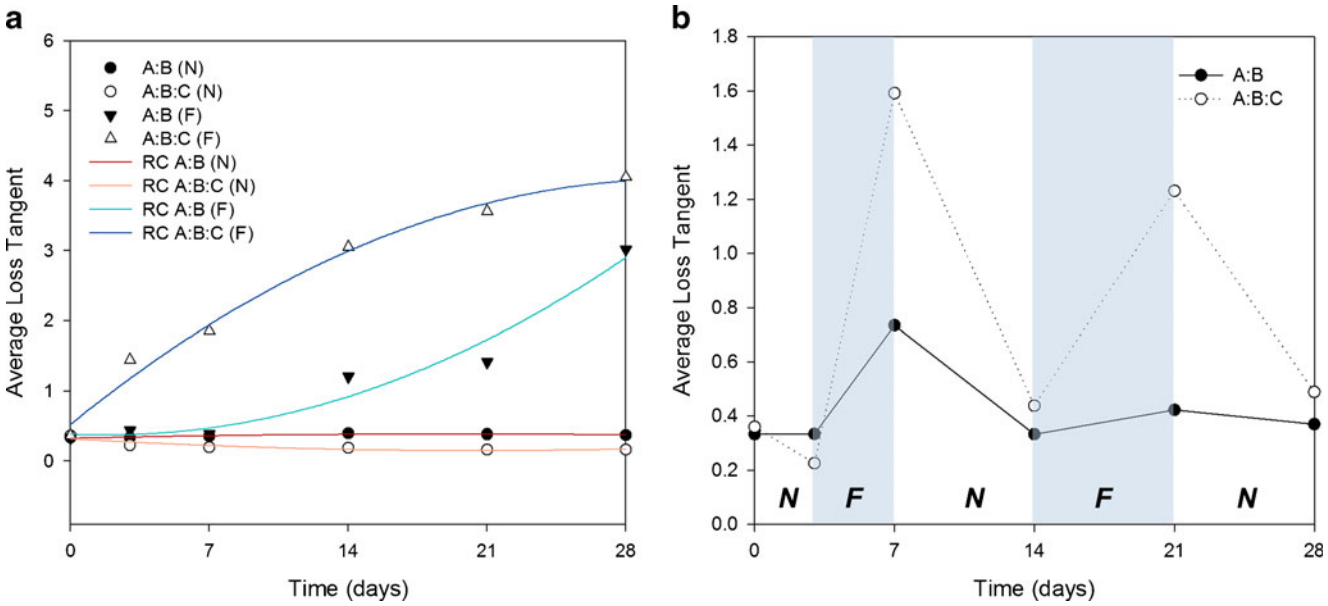

Fig. 2 (**a**) Frequency sweep results in constant normal or pathological media for the precursor SRHS combinations with associated regression curves (RC); (**b**) Frequency sweep results in alternating normal *vs*. pathological media for the precursor SRHS combinations. Note: The outer BPM SRHS is represented by *A*, the inner SRHS by *B*, and the initiator solution by *C*. A:B (outer: inner BPM SRHS) = 1 mL: 0.5 mL; A:B:C (outer BPM: inner BPM: initiator solution) = 1 mL: 0.5 mL: 0.1 mL. *N* normal conditions in SVH, *F* pathological conditions with Fenton's reagent in SVH.

Characterization of Vibrational Transitions by Fourier Transform Infrared Spectroscopy

Chemical Transitions of the Inner and Outer BPM, and BPM Interface

The observed chemical transitions for the outer BPM polymers, outer BPM, and inner BPM generated via FTIR analysis are compared in Fig. 3a and elaborated for the outer BPM in Fig. 3b. The final crosslinked BPMs showed the presence of bands characteristic to all its components, with a reduction in intensity of selected bands and the appearance of new bands, attributable to the intra- and intermolecular crosslinking initiated in the presence of the chemical crosslinkers and initiators, namely DCC and NHS in the outer core, and gluteraldehyde in the inner core, all of which migrate throughout the device during its formation. Summative bond designations are proposed in Table VI.

Thermal Analysis of the I^3

Characterization and comparison of pertinent thermal transitions, such as the T_g, of the native polymers and drugs, and the formed inner and outer BPMs was undertaken via TMDSC, as described under the "Materials and Methods", in order to define the degree of crosslinking within the I^3. The shift in the T_g of the inner and outer BPMs of the I^3, compared to the native polymers, as well as the corresponding predicted molecular weight between crosslinks, is provided in Table VII. The observed overall shift in the T_g of the I^3 compared to the unmodified polymers is predictive of a low molecular weight between crosslinks for the device.

On-Off Inflammation-Responsive Drug Release Capabilities of the Optimum Formulation

The I^3 formulation displayed adequate responsive capabilities on exposure to and removal of the inflammatory stimulus in terms of drug release, as exemplified in Fig. 4. A notably higher degree of drug release was achieved when implants were exposed to pathological conditions (hydroxyl radicals generated by Fenton's reaction). Ciprofloxacin was released to a greater extent due to its presence in the outer BPM, which is anticipated to erode at a faster rate, as well as its non-incorporation in a nano-carrier.

Magnetic Resonance Imaging for Live-Acquisition of the Inflammation-Responsive Transitions of the I^3

The approach of Tajiri *et al*. (27), which has been applied to hydrogel matrix tablets, was adapted to differentiate gelled (extensively hydrated) and non-gelled regions of the I^3 and the changes in hydration with time and on exposure to normal and inflammatory dissolution media. In each image, a lower degree of hydration or gelling of the I^3 is visualized as lower intensity, darker areas, whereas more extensive hydration or gelling of the implant possess an appearance falling towards the white side of the intensity scale (Fig. 4a). The high-intensity areas of the hydrogels in MRI images (white part) possess a smaller relaxation time (T_1) than bulk dissolution media (gray

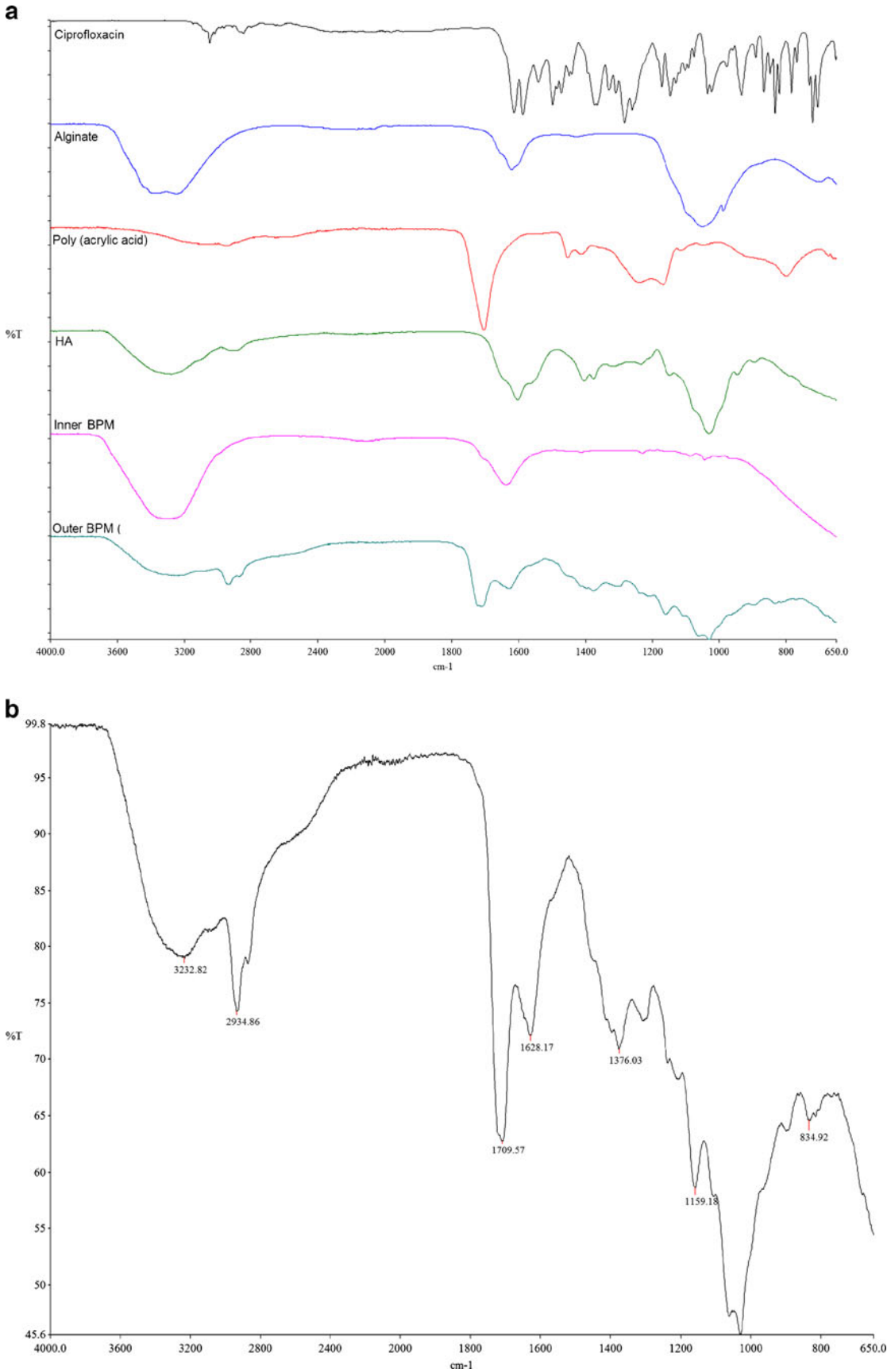

Fig. 3 (**a**) Comparative FTIR spectra of the native polymers, inner BPM, and outer BPM (**b**) Expansive FTIR spectrum of the crosslinked outer BPM.

region) due to the hydrogen bonds between the essentially hydrophilic polymers comprising the I^3 and water (27). The image of the I^3, which had not been exposed to dissolution media, is visualized in Fig. 5a. The MRI ^{1}H NMR images of the I^3 at subsequent stages of the dissolution test as visualized in the flow-through apparatus under normal, inflammatory and fluctuating conditions, are represented in Fig. 5b–d. Images highlight the enhanced hydration (with corresponding limited drug release) of the device under normal conditions, yet limited hydration (with erosion of the I^3 and comparatively enhanced drug release) under inflammatory conditions, exemplifying the stimulus-responsive behavior of the device.

Morphological Characterization and Image Processing Analysis of Erosional Behavior of the I^3

Image analysis was undertaken using mathematical software (Mathematica® v. 8.0, Wolfram Research Inc., Champaign, IL, USA) employing intermediate image-processing steps for enhancing image contrast (28), in order to describe the overall architecture and changes in morphological attributes of the inner and outer BPM following exposure to normal and inflammatory conditions. Through analysis of the image histograms generated, differences in transitions in morphological features on erosion of the device on exposure to normal and pathological dissolution media after 72 days, captured via SEM (raw images are depicted in Fig. 6), could be discriminated. Figure 7a for the erosion of the outer BPM under normal conditions shows a tetramodal distribution of peaks with four peaks at voxel intensities of ~25, 85, 160 and 200. For the erosion of the outer BPM on exposure to inflammatory conditions (Fig. 7b), a tetramodal distribution of peaks with voxel intensities at ~25, 70, 100, 150 was observed

Analysis of the erosion of the inner BPM under normal conditions revealed a pentamodal distribution at 20, 95, 170, 220 and 245 (Fig. 8a). For analysis of the erosional behaviour of the inner BPM under inflammatory conditions, a pentamodal distribution of peaks at ~27.5, 90, 110, 150 and 205 was apparent (Fig. 8b).

Quantification of the *In Vivo* I^3 Erosion and *In Vivo* Anti-Inflammatory and Antibiotic Concentrations Released from the I^3 into the Total Posterior Ocular Fluids of the Rabbit Eye Model Under Normal and Inflammatory Conditions

The gradient method employed proved successful for simultaneous detection of ciprofloxacin and indomethacin in rabbit posterior ocular fluid. Chromatographic analysis via UPLC revealed three separated and defined peaks at 318 nm at the respective retention times of 0.515 (nicotinic acid), 0.820 (ciprofloxacin), and 1.620 (indomethacin) minutes, in order of increasing lipophilicity (as the solvent program shifts towards a greater ACN ratio). Absolute recovery of indomethacin and

Table VI Bond Designations for the Outer Crosslinked BPM

Bond	Type of bond	Specific type of bond	Absorption peak	Appearance
C-H	Alkyl	Methyl	2930-2960 cm^{-1}	medium to strong
C=O	carboxylic acids/derivates	saturated carboxylic acids	1710 cm^{-1}	
	carboxylic acids/derivates	Amides	1650 cm^{-1}	
	alcohols, phenols carboxylic acids	carboxylates (salts)	1550-1610 cm^{-1}	
	primary amines	amino acid zwitterions	1550-1610 cm^{-1}	Broad
		high concentration		Strong
			3200-3400 cm^{-1}	multiple broad peaks
		amino acid zwitterions	1560-1640 cm^{-1}	
O-H	secondary amines ammonium ions	Any	2400-3200 cm^{-1}	Medium
	Alcohols	Tertiary	1150-1200 cm^{-1}	
		Any	1200 cm^{-1}	
N-H	primary amines	Tertiary	1120 cm^{-1}	
	phenols	Any aliphatic aromatic	1220-1260 cm^{-1}	two bands (distinct from ketones, which do not possess a C-O bond)
	Ethers	Any	1250-1300 cm^{-1}	often overlapped
	ammonium ions	Any	1100-1300 cm^{-1}	similar conjugation effects to C=O
C-O	carboxylic acids	Any	1020-1220 cm^{-1}	
	esters aliphatic amines	Any	1615-1700 cm^{-1}	

Table VII Thermodynamically-Derived Data for the I^3 (As the Inner and Outer BPM) Compared to the Native Polymeric Components

Relational Polymer	T_g-T_{g0}/ T_g (%)	M_c (gmol^{-1})	Difference in ΔH (Jg^{-1})
Outer BPM[a]			
ALG	95.74	407.35	101
HA	109.25	356.98	35.75
PAA	43.84	889.60	50.58
Inner BPM[b]			
Chitosan	9.65	4041.45	−35.59

[a] Compared to outer BPM thermal data

[b] Compared to inner BPM thermal data

ciprofloxacin from the TPOF samples by the liquid-liquid phase extraction process employed was performed by comparison of peak areas from extracted low and high calibration standards to those from aqueous standards. The recovery of both indomethacin and ciprofloxacin obtained during the extraction procedure spiked into blank TPOF samples from the non-test rabbit eyes ranged from 92.8 ot 97.4% for indomethacin and 95.4–101.6% for ciprofloxacin, indicating acceptable methodological conditions for evaluation of drug concentrations in the TPOF of the rabbit eye model. Calibration curves generated for both indomethacin and ciprofloxacin were satisfactory.

Following sub-Tenon implantation of the drug-free and drug-loaded I^3 in two groups of 10 rabbits ($n=5$), intraocular inflammation was successfully induced in the inflamed rabbit eye group via intravitreal injection of *Salmonella typhimurium* LPS into the I^3-implanted eye. On day 7, all rabbits were euthanized, the implanted eye was enucleated with removal of the device, and the central vitreous humor aspirated and stored with the isolated

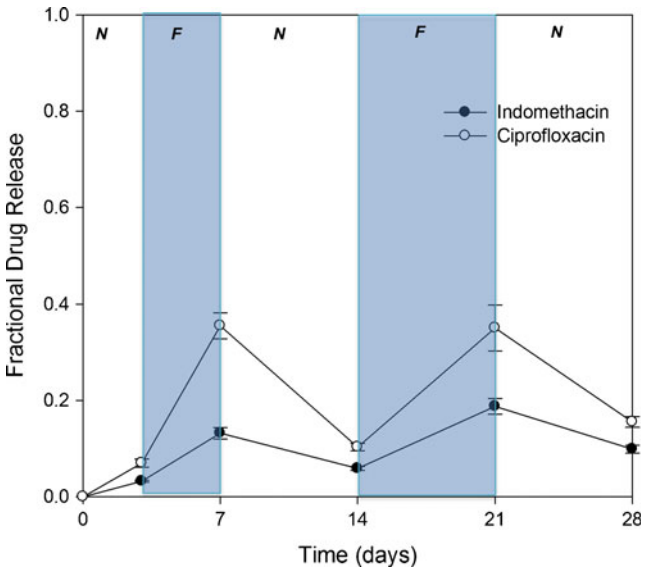

Fig. 4 Drug release profiles signifying the on-off inflammation-responsive capabilities of the optimum formulation. *N* normal conditions in SVH, *F* pathological conditions with Fenton's reagent in SVH.

orbital tissues for subsequent analysis of the TPOF. The seven-day ocular levels of both indomethacin and ciprofloxacin were then measured. Figure 9a highlights the removal of the I^3, which was isolated intact at day 7 from both the normal and inflamed rabbit eye, prior to enucleation for vitreous and tissue sampling. There was enhanced release of both drugs in the inflamed rabbit eye even after 7 days, with indomethacin levels of 0.749 ± 0.126 μg/mL and 1.168 ± 0.186 μg/mL, and ciprofloxacin levels of 1.181 ± 0.150 μg/mL and 6.653 ± 0.605 μg/mL being attained in the normal and inflamed eye, respectively (Fig. 9b). Furthermore, the enhanced erosion of the I^3 in the inflamed eye is also exemplified (Fig. 9b), with the I^3 eroding 1.504 ± 0.505% in the normal eye and 22.609 ± 2.421% in the inflamed eye after 7 days.

Histomorphological Analysis for Assessment of the Degree of Ocular Inflammation Following Implantation of the I^3 in the Normal and Inflamed Rabbit Eye

Histomorphological evaluation of the ocular milieu, the I^3 biocompatibility and biodegradability, and associated degree of inflammation was undertaken on all representative samples. Table VIII and the associated Fig. 10 (at magnifications which were the best representation for that section) exemplifies the levels of anterior and posterior inflammation present in the control rabbit eye (where no inflammation was induced or implant inserted), following of induction of inflammation, and following implantation of the drug-free and drug-loaded I^3 in the normal and inflamed rabbit eye. Histological assessment of cellular infiltrates revealed that the degree of posterior inflammation in the inflamed rabbit eye in which the drug-loaded I^3 was implanted was notably less (1+ grading) than that observed in the inflamed eye receiving a drug-free device (3+ grading), indicating a corresponding positive physiological response to the enhanced drug levels observed in the inflamed rabbit eye.

DISCUSSION

Molecular Modeling Simulations for Prediction of Pertinent Interactions between the I^3 and Normal or Inflammatory Milieu

As indicated under the "Results" of the *in silico* modeling undertaken (Eqs. 8–13), the final optimized solvated architectures for the bipolymeric architectures were destabilized as compared to the monopolymeric (individual) molecules under similar conditions. This structural destabilization may lead to dislodgement of individual polymers from the bipolymeric complex in order to stay as stabilized as the monopolymeric form in the solvated system. This very tendency of the polymers to stay in their original conformation rather than in

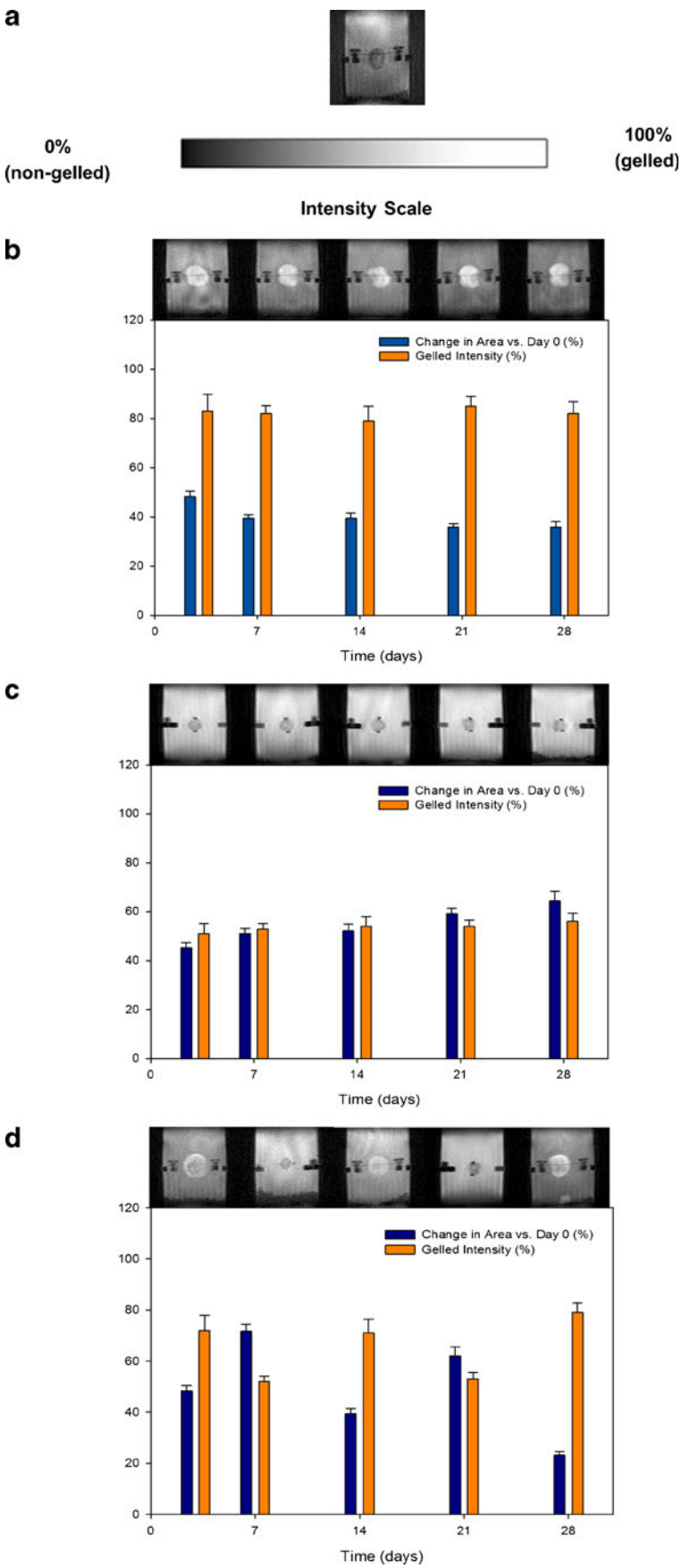

Fig. 5 (**a**) MRI of the I^3 at day 0 and the intensity scale highlighting gelled and non-gelled areas; (**b**) Graphical depiction and associated MRIs exemplifying hydration transitions of the I^3 over 28 days in normal SVH; (**c**) Graphical depiction and associated MRIs exemplifying hydration transitions of the I^3 over 28 days in Fenton's Reagent in SVH; and (**d**) Graphical depiction and associated MRIs exemplifying hydration transitions of the I^3 over 28 days in alternating media.

complex form might lead to the separation of the polymers after implantation, hence affecting the performance of the polymeric system. Interestingly, the tripolymeric system demonstrated a substantial decrease in energy values with all the non-bonding energy components working towards the structural stabilization (Eq. 14). This minimization was rendered due to enhanced H-bonding (Fig. 1a) and electrostatic interactions which led to the formation of an intact complexed structure capable of acting in conjugation. The tripolymeric structure of the outer BPM thus has a good propensity to maintain its patency under normal ocular conditions.

The inherent focus of this study was to fabricate an inflammation-responsive polymeric system for stimuli-modulated ocular delivery of one or more drugs. In addition to the above simulations in water; a modeling simulating a pathological inflammatory intraocular state created in the presence of hydroxyl radicals was also performed to elucidate the effect of the inflammatory agents on the polymers, specifically the HA molecule. The $OH^{\cdot}$-mediated stimuli-responsive behavior of the outer BPM can be accredited to the action of the $OH^{\cdot}$ on specific bonding/ functional sites on the polysaccharides as displayed in Fig. 1b and c. The MMER analysis confirmed the interaction potential of the hydroxyl radicals with polysaccharides in terms of both HA (Eqs. 9 and 15) and the tripolymeric structure (Eqs. 14 and 16). The complexes were hugely stabilized by ion pair-ion pair electrostatic non-bonding interactions. All other bonding and non-bonding interactions contributed to the destabilization of the structure proving the dominating role played by the ionized species. These energy attributes may indicate activation barriers for the first stage (abstraction of the hydrogen on the carbon adjacent to the carboxyl group in the *n*-glucuronic acid unit, leading to glycosidic cleavage) and second stages (formation of a hydrolytic product) (26). As can be deduced from the geometric configuration, the volume of polysaccharide fractions as well as the solvent-accessible surface obviously decreases during the catalytic process. This decrease in molecular size can be related to the ordering of polysaccharide fractions, which is usually accompanied with a lowering in steric energy (32). This ordering conformation provided clear evidence for the catalytic effect of the hydroxyl radicals in HA hydrolysis. The activation barriers of these reactions were lowered. In addition, the main forces that may cause the change of molecular size were analyzed by the final single point energies. Van der Waals and hydrogen bonding energies increased significantly; whereas this was not the case for electrostatic energy during the simulation process. These findings were fully in agreement with the results that van der Waals attraction, hydrophobic forces, and electrostatic interactions were the dominant driving force in the formation of an ordered polymer structure (33). In general, the more negative the force energy is, the more thermodynamically favorable is the formation of the ordered structure. The change in bonded interaction was exothermal as can be determined from the enthalpy change (negative) indicating that the bonded interaction may also accelerate the hydrolysis of saccharide molecules.

Oscillatory Studies: Frequency Sweep Tests

Oscillatory studies were important in demonstrating the stimulus-responsive rheological transitions of the SRHS forming the BPMs. Figure 2a highlights that the interaction between the functional groups was disrupted in the Fenton's Reagent as compared with the normal SVH, as highlighted by the respective regression curves. The decreased interactions between the multipolymeric functional groups would purportedly facilitate enhanced erosion of the final BPMs under inflammatory conditions compared to normal conditions, fulfilling the purpose of inflammation-responsiveness.

In the presence of Fenton's Reagent, the solution displayed average loss tangent values of greater than 1 (Fig. 2b). It can therefore be assumed that in response to inflammation, interpolymeric interactions are decreased and the ultimate system elasticity is reduced. This may be advantageous in allowing for surface erosion and hence the release of drug. Rheological synergism was observed in A:B:C (34). This synergism is typically a result of hydrogen bonding interactions between the polymer chains facilitated by the compatible geometries of the interacting polymers (35).

Characterization of Vibrational Transitions by Fourier Transform Infrared Spectroscopy

Chemical Transitions of the Inner and Outer BPM, and BPM Interface

The resultant FTIR spectrum is a predictor of the type of bond formed during the polymeric crosslinking, with specific reference to HA (Fig. 3a and b). The additional band at 2,934 cm^{-1} points to the presence of additional alkyl chains on HA, ALG and PAA corresponding to -CH and -CH_2 vibrations (36), introduced in the presence of DCC and NHS. This could indicate both intramolecular and intermolecular crosslinking within the polyanions themselves, as well as between HA, ALG, and PAA. The participation of ALG and PAA in forming an intricately crosslinked structure is evident by the appearance of bands at 1,628 cm^{-1} and 1,159 cm^{-1} representative of the ester functionality, being a pertinent indicator of intra- and intermolecular crosslink formation.

An interpenetrating network at the site of conversion at the inner and outer BPM is anticipated to form between the cationic chitosan amino groups and the anionic ALG, HA and PAA carboxylic groups, potentially disrupting any hydrogen bonding already present between amino groups and hydroxyl groups in CHT and elaborating an amorphous structure. Even though the

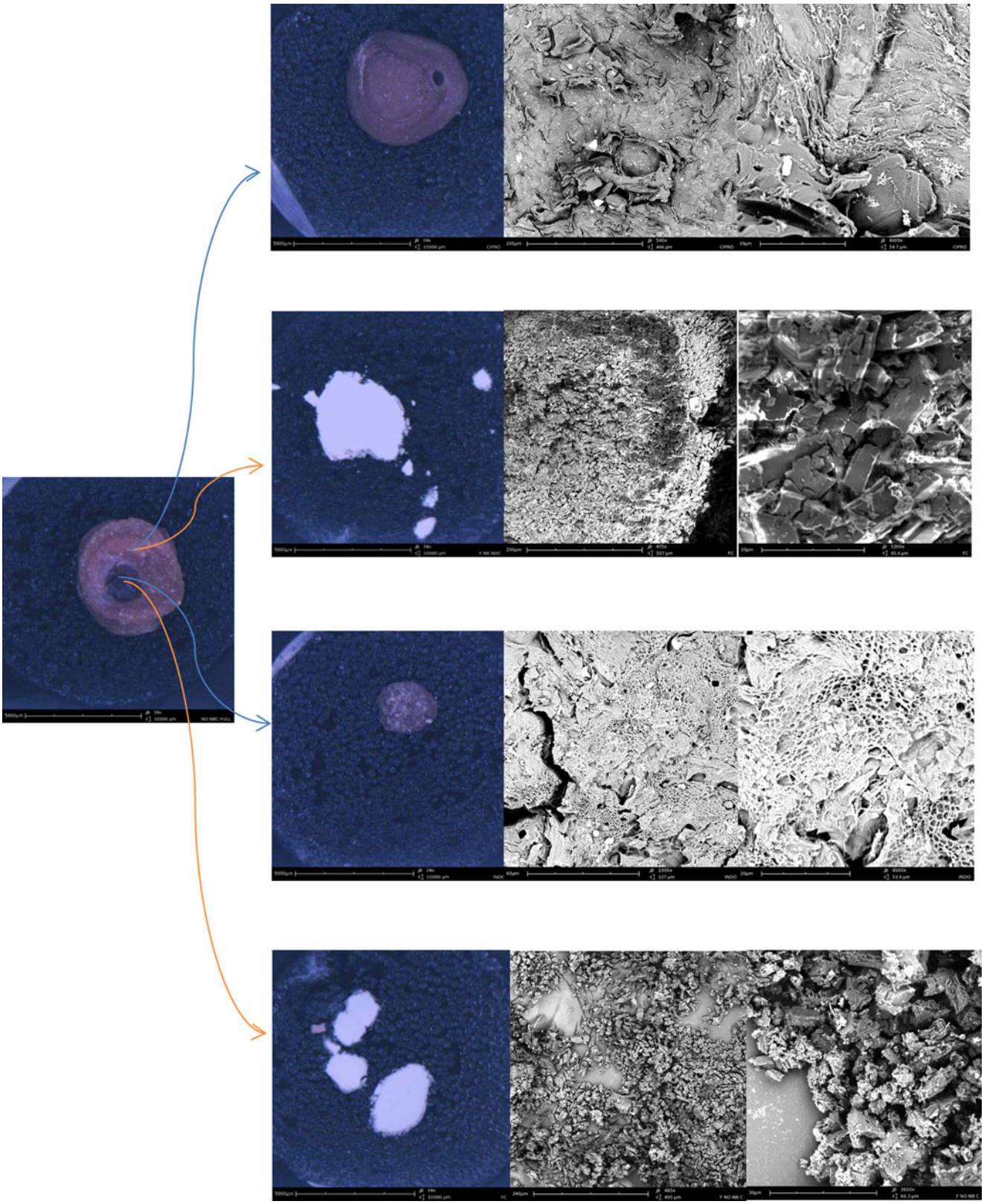

Fig. 6 Componentially-derived scanning electron micrographs of the outer and inner BPMs under normal (*blue arrow*) and inflammatory (*orange arrow*) *in vitro* conditions after 72 days exposure (represented at incremental magnifications).

inner and outer BPM are evident as separate entities, there is integration of chitosan into the outer BPM at the boundary and the crosslinking interaction between these entities is visualized in the FTIR spectrum of the outer BPM. The occurrence of a new

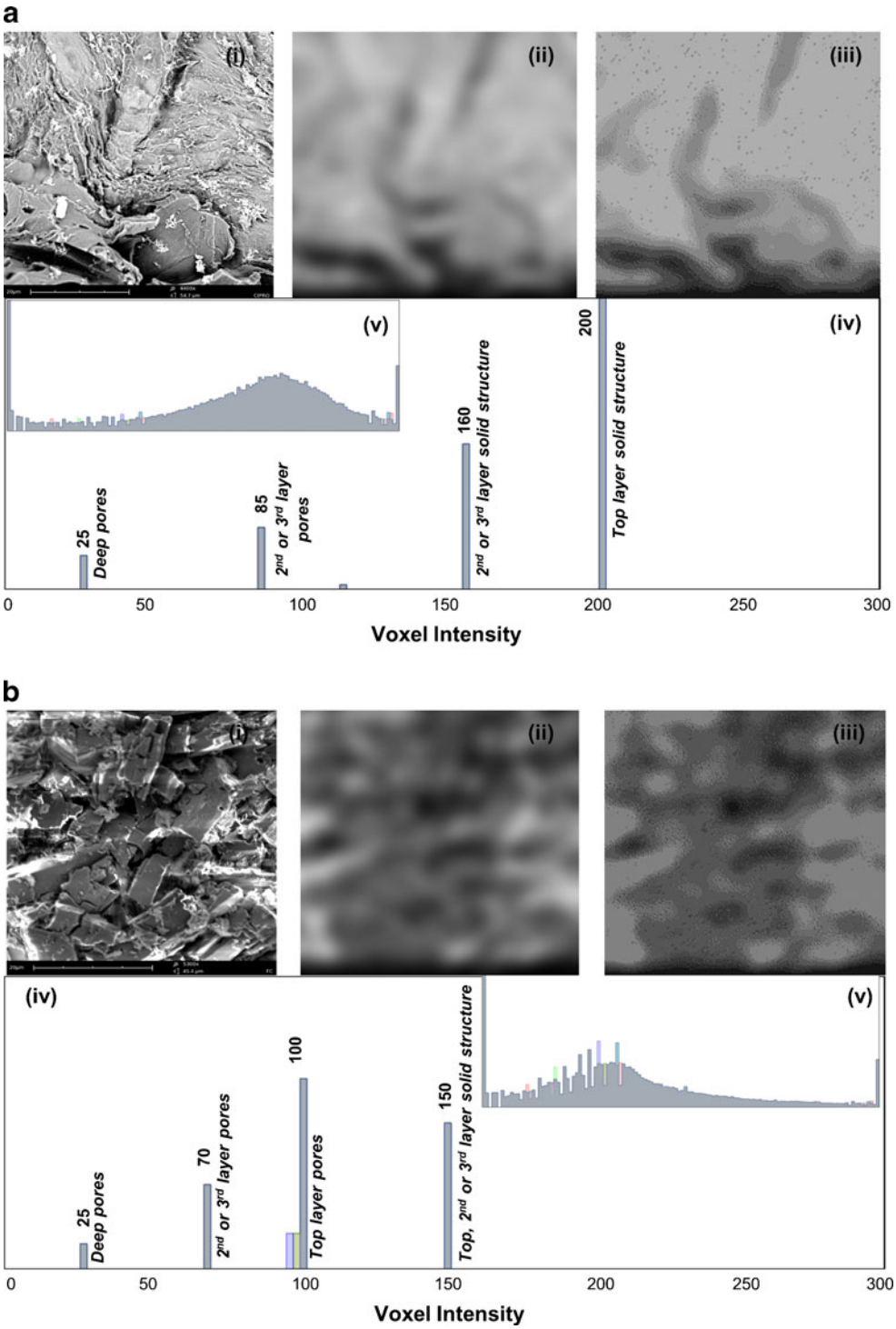

Fig. 7 Image processing with subsequent (*iv*) image histograms generated for high-magnification images of the outer BPM, showing proposed peak designations, and (*v*) the histogram of the original SEM shown as an inset, under (**a**) normal and (**b**) inflammatory conditions showing the (*i*) original, (*ii*) blurred, and (*iii*) color quantized image. Note that each channel is capable of highlighting most of the pores and layers but not all.

band at 3,232 cm^{-1} is representative of ionization of amine groups. This corresponds with a comparative increase in intensity in the peak at 1,650 cm^{-1}, indicating the carbonyl group of amides. The increase in intensity of the peak at 1,630–1,650 cm^{-1} are characteristic of the C = N group, which confirms the formation of Schiff's linkage, corresponding to ionic interactions between chitosan and the polyanions such as HA (37).

With regard to the inner BPM (Fig. 3a), previous reports have shown that most substantial changes in the spectra of crosslinked CHT occur in the absorption region of CH_2 groups (3,000–2,800 cm^{-1}) and aldehyde, amide, and amino groups (1,700–1,300 cm^{-1}) (38,39). The presence of the azomethin group in the product of reaction of chitosan with gluteraldehyde is easiest to follow from the peak of valence vibrations of the C = N bond which appears in the region of

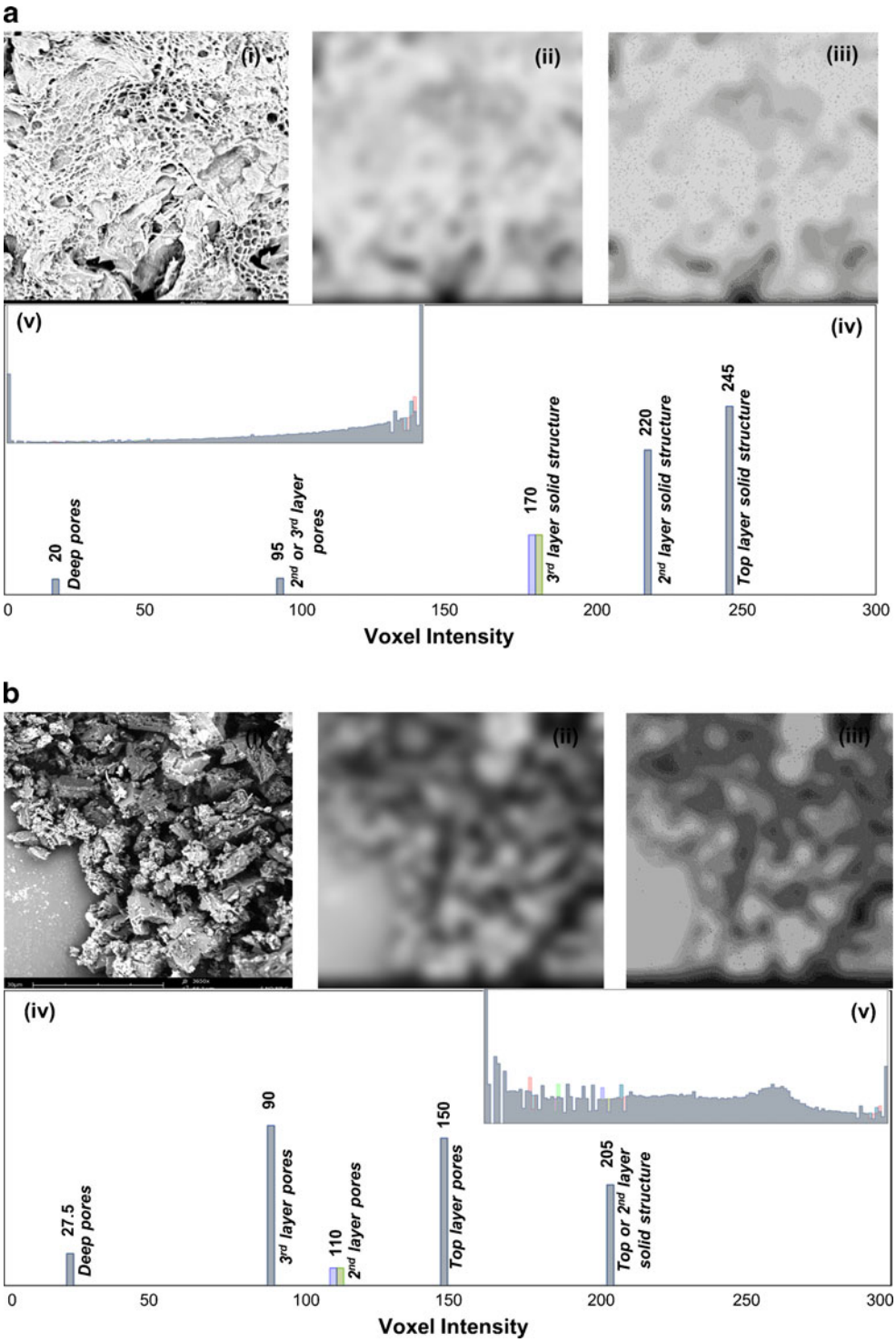

Fig. 8 Image processing with subsequent (*iv*) image histograms generated for high-magnification images of the inner BPM, showing proposed peak designations, and (*v*) the histogram of the original SEM shown as an inset, under (**a**) normal and (**b**) inflammatory conditions showing the (*i*) original, (*ii*) blurred, and (*iii*) color quantized image. Note that each channel is capable of highlighting most of the pores and layers but not all.

1,680–1,620 cm^{-1}. These products appear during the crosslinking of CHT. The formation of the aldimine bond activates the added gluteraldehyde molecule and accelerates the elongation of the oligomeric chain of gluteraldehyde on chitosan. This is evidenced by the appearance of a band of valence vibrations of aldehyde groups in the IR spectra of the products of the reaction of CHT and gluteraldehyde at ~1,706 cm^{-1}. Further transformations with the formation of the already crosslinked product can occur through the condensation of the amino groups of chitosan with the carbonyl groups of modified chitosan, or through the aldol reaction and condensation of oligomeric chains of modified chitosan with the formation of the products.

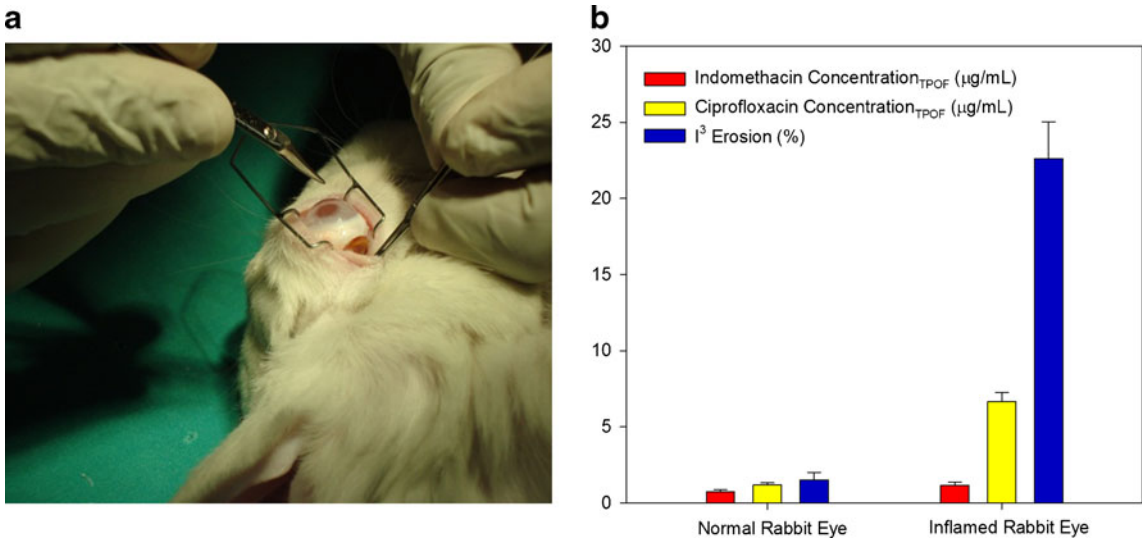

Fig. 9 (**a**) Photographic image highlighting removal of the I^3 from the rabbit eye at day 7 prior to enucleation for vitreous and tissue sampling. (**b**) Drug levels and I^3 erosion measured at 7 days in the posterior ocular fluids in the normal and inflamed rabbit eye.

Table VIII Levels of Anterior and Posterior Inflammation Observed Following Inflammation Induction and I^3 Implantation at 7 Days

Ocular Specimen	Anterior Inflammation	Posterior Inflammation	Additional Observations	Histological Image (Figure 10)
Control	0	0	Normal morphology without any inflammation visible in the anterior and posterior chambers.	(a)
LPS Injection	1+	3+	Acute purulent panopthalmitis could be confirmed with severe exudation into the posterior chamber and vitreous humor as well as mild inflammation visible in the anterior chamber of the eye. Polymorphonuclear leukocytes (heterophils) appeared to predominate in the exudative inflammatory process, but some mononuclear leukocytes as well as macrophages were scattered in the protein-rich inflammatory exudate. Additionally, cell debris and desquamated epithelium cells were observed in the vitreous material. The exudate extended up to the retina and was also present in the ciliary processes, but did not penetrate into the sub-epithelial stroma.	(b)
Drug-free I^3—normal eye	0	0	Normal anatomical features are observed in the intraocular structures as well as the sclera and extraocular soft tissues.	(c)
Drug-loaded I^3—normal eye	0	0	No intraocular pathological changes with no specific lesions present in the soft tissues around the eyeball in these sections	(d)
Drug-free I^3—inflamed eye	1+	3+	At day 7, acute exudative panopthalmitis was detected where heterophils and fibrin exudation were found in the anterior and posterior (vitreous) chambers of the eye. A section from the optic nerve highlighted lymphocytic perivascular cuffing within the optic nerve where prominent lymphoplasmacytic infiltrates were found around some of the capillaries in the nerve.	(e)
Drug-loaded I^3—inflamed eye	0	1+	A mild exudative inflammation was demonstrated in the posterior chamber and in the vitreous chamber of the eye. The intraocular inflammatory process appeared acute and mild. Polymorphonuclear leukocytes (heterophils) predominated with some protein-rich fibrinous exudate also present. The anterior chamber of the eye was clear of any inflammatory infiltrates. The exudative panopthalmitis was visualized as mild and acute in the posterior vitreous chamber of the eye. The subacute inflammation on the extraocular stroma was graded as mild.	(f)

0 no detectable inflammation, *1+* mild inflammation, *2+* moderate inflammation, *3+* severe inflammation, *LPS* lipopolysaccharide

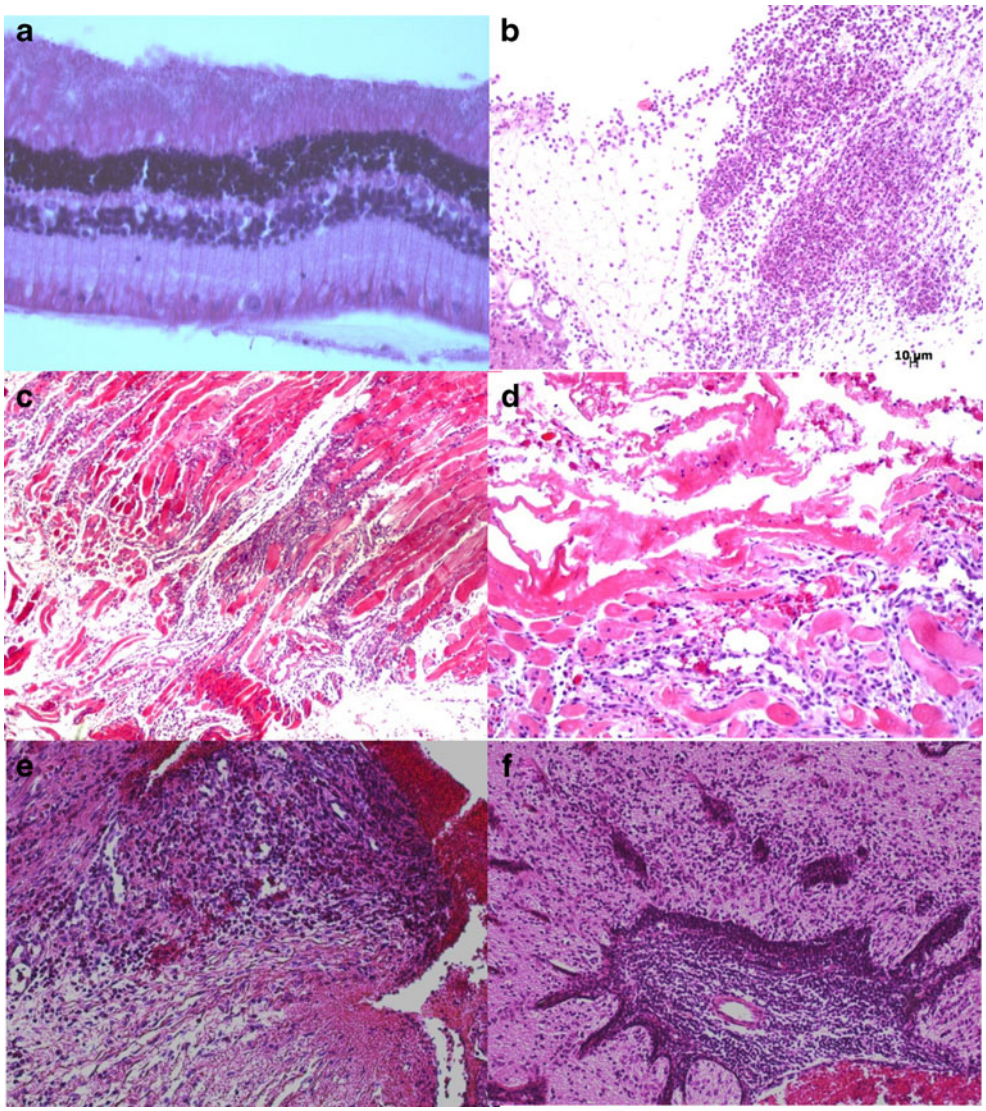

Fig. 10 Histological slides at day 7 for (**a**) the control eye showing the normal retina at 10x magnification (**b**) LPS injected eye at 10x magnification (**c**) drug-free I^3 in the normal eye at 4x magnification (**d**) drug-loaded I^3 in the normal eye at 20x magnification (**e**) drug-free I^3 in the inflamed eye at 10x magnification and (**f**) drug-loaded I^3 in the inflamed eye at 10x magnification.

Comparison of the IR spectra of pristine and glutaraldehyde-crosslinked CHT revealed significant transitions. The crosslinking of chitosan membranes with glutaraldehyde shows that an increase in the absorption at ~1,655 cm^{-1} is seen due to imine bonds (N = C). The slight shoulder at 1,720 cm^{-1} is due to free-aldehydic bonds. There is a high intensity broad peak extending from 3,500 to 2,900 cm^{-1}, which could be attributed to the N-H and hydrogen bonded O-H stretch vibrational frequencies (at 3,431 cm^{-1} in pure chitosan) and an increase in the intensity of the C-H stretch increase at ~2,936 cm^{-1}. The increase in the number of methylene groups in the products of condensation of chitosan and gluteraldehyde is known to manifest itself as changes in the ratio of band intensities in the region of 3,000–2,800 cm^{-1} (39). The intensity of the peak at ~1,100 cm^{-1} attributed to the presence of the aliphatic amino group is decreased drastically in the crosslinked BPM compared to native CHT. This change pertinently highlights that the crosslinking with glutaraldehyde transforms the membrane to a more hydrophobic form as amino groups are blocked with aliphatic chains (37).

Thermal Analysis of the I^3

Thermal analysis via TMDSC was significant in characterizing the degree of crosslinking of the BPMs forming the I^3. Overall, there was a significant shift in the T_g in the I^3, represented as the outer and inner BPM, compared to the native components. This is a predictor of the numerically predicted low molecular weight between crosslinks, relationally ascribed to each polymeric contributor, as provided in Table VII. Simply, this was further redolent of a highly crosslinked structure, even with regard to CHT which already has a high T_g. The difference in ΔH at the glass transitions for each polymer compared to the I^3 was also calculated—the larger the difference, the more energy required to induce thermal transitions i.e. metamorphosis from a glassy to rubbery state, melting and ultimately thermal degradation,

which was clearly the case for the multipolymeric device compared to its polymeric constituents.

On-Off Inflammation-Responsive Drug Release Capabilities of the Optimum Formulation

The drug release pattern obtained from the I^3 was differential in normal *versus* pathological (inflammatory) conditions (Fig. 4), with reversibility demonstrated *in vitro* (even though a degree of loss in the bioresponsive capabilities of the device with time is anticipated as irreversible changes in the polymeric integrity of the I^3 will ultimately occur as chain scission is repeatedly initiated in the presence of hydroxyl radicals). The enhanced release of both drugs under inflammatory conditions is attributed to the stimulated surface erosion of the inflammation-responsive BPMs, specifically the encapsulating outer BPM, as predicted via *in silico* modeling.

Under normal conditions, an initial low level release of both drugs from the I^3 was still observed. The initial presence and continued pore formation is a possible anticipated mechanism contributing to this. Porosity analysis undertaken (Supplementary Table I) indicated that for the outer BPM, the pore size is much larger compared to the inner BPM, which exhibits a smaller pore size overall. This clearly exemplifies that, in the inner BPM, the pores are essentially occupied to a great extent by the NS, thus having an enhanced surface area (availed by the NS and numerous small pores), whereas in the outer BPM, the pores are larger, possessing a smaller surface area. On initial exposure of the I^3 to dissolution media, the pores of the outer BPM are anticipated to enlarge under normal conditions causing ciprofloxacin release and the release of indomethacin-loaded NS located at the boundary of the inner and outer BPM, which is reflected in the early phase release of low levels of indomethacin and slightly higher levels of ciprofloxacin. Indomethacin release could also be attributed to release of NS or indomethacin dissolution from the embedded NS located at the exposed surface of the inner BPM.

An inflammation-responsive drug release approach not been demonstrated for intraocular implants on the market for the treatment of posterior segment inflammation, such as the market leader, Retisert™. The Retisert™ provides continuous delivery of the corticosteroid (6). Because there is continuous release of anti-inflammatory drug, irrespective of the presence or absence of inflammation, there is an enhanced propensity for the occurrence of side effects. This would be minimized from the proposed system which provides enhanced drug release when exposed to an inflammatory stimulus compared to when the implant is subjected to normal intraocular conditions.

Magnetic Resonance Imaging for Live-Acquisition of the Inflammation-Responsive Transitions of the I^3

MRI was undertaken to demonstrate the variability in gelling of the device in the presence and absence of the inflammatory stimulus, which was importantly correlated with the drug release behavior from the I^3. Plotted results indicate the gelled intensity (i.e. the intensity of the white area of the I^3, which is the hydrated area), as well as the change in area of the I^3 on exposure to the various dissolution conditions compared to the unhydrated I^3 at day 0. The associated MRIs at each time point are also provided. Upon initial inspection at day 0, the I^3 was clearly observed as a small unhydrated device in accordance with the associated intensity scale (Fig. 5a). Following exposure to normal SVH a comparatively greater imbibement of dissolution fluid occurred (indicated by the largely white appearance of the implant corresponding to a high gelling intensity in the MRIs in Fig. 5b). As drug release studies undertaken at normal conditions concluded, drug release was at a minimum highlighting that fluid uptake in this instance enforces the crosslinked structure emanating in a highly interconnected multipolymeric hydrogel which hinders drug and NS diffusion out the gel. Following exposure to SVH, compared to the device at day 0, there is a prominent increase in the area of the I^3. This is due to swelling caused by the high concentration of charged ionic groups in the crosslinked multipolymeric structure due to osmosis and charge repulsion. The overall hydration of the implant is apparent with the gelling intensity being consistently >~79% over 28 days. Thereafter, the slight progressive decrease in the size of the gel with time is indicative of a low degree of erosion occurring at the implant surface. Drug release observed under these conditions is most likely attributed to self-diffusion initially, followed by matrix erosion as the device area decreases. Fluid ingress with device hydration, causing an initial increase in the area of the implant with subsequent limited erosion over the investigated period, can be considered as a significant predictor of the drug release profiles of the I^3. The change in the device area decreased with time, concurrently with a limited increase in both indomethacin and ciprofloxacin release ($R^2 = -0.8856$, and $R^2 = -0.8783$, respectively). The high degree of device hydration (measured as gelling intensity) was thus important for limiting the drug release under normal conditions.

Subsequently, the transitions in the device' area and gelling intensity was measured for the implant under pathological conditions created by Fenton's reagent in SVH (Fig. 5c). Ingress of fluid was minimal in Fenton's reagent, as evidenced by essentially a lower gelling intensity ranging between ~51 and 56% (with I^3 images appearing grey), however, there was a notable decrease in area with time, which corresponds with the predicted surface erosion of the device under inflammatory conditions due to chain scission initiated in the presence of hydroxyl radicals propogating the observed surface erosion

of the device. There is limited overall hydration of the device highlighting that the polymeric degradation initiated by the free radicals is largely a surface phenomenon. The change in the area of the implant increased with time and correlated positively and significantly with the observed drug release of both indomethacin and ciprofloxacin, with progressively increased erosion or the I^3 resulting in enhanced drug release ($R^2=0.9695$ and 0.9888, respectively).

The behavior of the I^3 on exposure to alternating dissolution stresses is of importance in that the 'on-off' inflammation-responsive transitions of the device become quite evident (Fig. 5d). In the absence of the instigating stimulus (hydroxyl radicals), from days 0–3, the I^3 hydrates and gels, visualized as a high gelling intensity; and the device area increases. On exposure to inflammatory conditions from day 3–7, device hydration decreases and chain scission is initiated at the surface of the I^3 with the implant area drastically decreasing. Under normal conditions from days 7–14, fluid ingress into the device progresses further into the core. After exposure to hydroxyl radicals for another 7 days, there was a noted decrease in the size and hydration of the device once again. Interestingly, after a further 7 days exposure to normal conditions, prominent hydration of the implant occurs; the device area does again increase, although not as notably as before, due to more extensive device erosion with pieces of the implant. This reversible swelling and gelling and then 'collapsing' of the polymeric matrix on alternating exposure to and removal of the instigating stimulus is a hallmark of stimulus-responsive systems (4). In this instance, collapse of the gel occurs in the presence of inflammation, which promotes erosion of the device. It is thus apparent that although the responsive behavior is reversible, a point is reached at which excessive stresses and polymeric chain scission may alter the mechanism of operation of the device to a degree. Large decreases in area of the implant were observed following exposure of the device to pathological conditions (subsequent to normal conditions) attributed to erosion in the presence of hydroxyl radicals with associated drug release. The correlation obtained between changes in device area and drug release was not remarkable for indomethacin ($R^2=0.5049$), but somewhat notable for ciprofloxacin release ($R^2=0.7375$), possibly due to the fact that ciprofloxacin was directly incorporated within the stimulus-responsive matrix; whereas following NS release from the eroding implant, indomethacin has yet to diffuse through its encapsulating boundaries.

Morphological Characterization and Image Processing Analysis of Erosional Behavior of the I^3

Image process analysis in accordance with the described method enabled differentiation of certain morphological features of the BPMs comprising the I^3 following exposure to either normal or inflammatory conditions. The comparative analysis of histograms, with the histogram of the original SEM shown as an inset to the histogram obtained after image processing, highlighted the effect of the processing steps on the clarity of the image histogram such that the respective erosional effects on BPM morphological features could be distinguished. Figure 7a for the erosion of the outer BPM under normal conditions shows a tetramodal distribution of peaks with four of the peaks at voxel intensities of ~25, 85, 160 and 200 representing voxels for air-filled deep pores, pores reaching the second or third layer of the structure, solid polymeric architecture in the second or third layer of the structure, and the solid polymeric architecture of the top layer, respectively, in the order of increasing linear absorption coefficients. The black regions visualized in the processed images are representative of deep pores, cracks and crevices extending from the surface into deeper layers of the respective BPMs of the I^3 which become enlarged on erosion. The peaks on either side of these pores and solid interfaces are blurred because of the finite spatial resolution of the scanning system instigating an undesirable partial volume effect. The probability of finding intensity at a pore-solid polymer boundary was assumed to be equal for both features. The average of these peaks was thus established as the threshold (i.e. ~118) implying that voxels with an intensity equal to or smaller than 118 are pores, which is true for the peaks at 25 and 85, which were assumed as pores initially. This model was used for comparison with the images acquired for exposure of the outer BPM to inflammatory conditions (Fig. 7b). Here there was a tetramodal distribution of peaks with voxel intensities at ~25, 70, 100, 150, representing a significant shift towards a more porous structure on exposure to an inflammatory environment.

Analysis of the erosion of the inner BPM under normal conditions revealed a pentamodal distribution at 20, 95, 170, 220 and 245, representing voxels for air-filled deep pores, pores reaching the second or third layer of the structure, solid polymeric architecture in the third layer, solid polymeric architecture in the second layer of the structure, and the solid polymeric architecture of the top layer, respectively (Fig. 8a). The threshold was thus established at ~150, implying that pores are represented by peaks at or below this intensity. Thus, under normal conditions, the more solid architecture is attributed to the fact that the NS still occupies a great deal of the pores of the matrix until their ultimate dislodgement from the system on matrix erosion. When exposed to inflammatory conditions, analysis of the SEM image of the inner BPM highlighted a pentamodal distribution of peaks at ~27.5, 90, 110, 150 and 205, indicating a highly porous matrix with excessive loss of the embedded NS (Fig. 8b). The inner BPM

was resolved into more layers than the outer BPM (pentamodal *vs*. tetramodal) due to pores arising which were artefacts of NS release from the matrix.

Quantification of the *In Vivo* I^3 Erosion and *In Vivo* Anti-Inflammatory and Antibiotic Concentrations Released from the I^3 into the Total Posterior Ocular Fluids of the Rabbit Eye Model Under Normal and Inflammatory Conditions

In vivo results generated via UPLC analysis of TPOF samples demonstrated good penetration of drug from sub-Tenon's space, through the sclera, into the TPOF, with drug levels being above the minimum effective concentration (MEC) of indomethacin (0.225 μg/mL) and minimum inhibitory concentration (MIC) of ciprofloxacin (0.8 μg/mL). *In vivo* results further emphasized the greater modulation of indomethacin release from the I^3 (as compared to ciprofloxacin) owing to its incorporation within the NS, enabling a more targeted and prolonged effect of the anti-inflammatory agent (Fig. 9b). This was congruent with *in vitro* observations.

Very few studies report on the inflammation-responsive behavior of implants; however the investigation of Yui *et al*. (40) on the inflammation-responsive degradation of crosslinked HA revealed erosion of 5–55% at 175 h (~7 days) at Fenton's reagent concentrations of 0.01–0.05 M. There was no comparator under normal conditions, and no drug was included for comparison with our data on inflammation-responsive drug release patterns. The degree of erosion of the I^3 at the same Fenton's reagent was half that described as 'rapid [responsive] degradation' by Yui *et al*. (40), highlighting a more controlled erosion due to the intimately crosslinked system. However, the erosion of the I^3 under inflammatory conditions was notably greater than that observed in a normal ocular milieu.

Histomorphological Analysis for Assessment of the Degree of Ocular Inflammation Following Implantation of the I^3 in the Normal and Inflamed Rabbit Eye

Histomorphological analysis of cellular infiltrates as a measure of the degree of inflammation concluded that the morphological findings in several sections where drug-loaded and placebo implants were left for 7 days in the sub-Tenon's space in the normal rabbit eye showed no morphological differences between the two groups (Fig. 10). The mild inflammation on the external surface of the sclera observed in some of the rabbit eyes appeared subacute and was associated with the I^3 in the sub-Tenon's space.

In the inflamed rabbit eye specimens, inflammation suggesting an acute, intraocular panopthalmitis could be confirmed in all of the sections with polymorphonuclear leukocytes (heterophils) predominating (Fig. 10b, e and f). This is a by-product of the inflammation that was induced via LPS injection. In the drug-free specimens a lymphocytic optic neuritis was confirmed (Fig. 10e). Because no drug was present in this instance, there was no opportunity for a reduction in the inflammation induced as opposed to where there was implantation of a drug-loaded device and a relatively high level of posterior inflammation was still detected (3+ grading). However, with a drug-loaded implant in the inflamed rabbit eye, morphological evaluation revealed only mild intraocular heterophil infiltrates in the vitreous chamber (1+ grading) with no inflammation in the anterior portion of the eye (Fig. 10f). This highlights a reduction in level of induced inflammation attributed to adequate site-specific release of drug (indomethacin and ciprofloxacin) from the I^3 in the presence of inflammation, and proves the efficacy of the I^3 in commencing to counteract the pathological tissue changes that occur when ocular inflammation is instigated.

CONCLUSION

Modeling simulating a normal as well as pathological inflammatory intraocular state (created in the presence of hydroxyl radicals) was performed for elucidation of the effect of the inflammatory agents on the polymers. The stimulus-responsive behavior of BPMs can be attributed to the action of the hydoxyl redicals on specific bonding/ functional sites on the polysaccharides forming the I^3. The MMER analysis confirmed the interaction potential of the hydroxyl radicals with the polysaccharides. *In silico* analysis also rationalized the use of a tripolymeric structure in the outer BPM. The intricately crosslinked polymeric system comprising the I^3 thus responded at an innate level predicted by its molecular make-up to inflammatory conditions as indicated by the results of the rheological analysis, MRI and SEM imaging, as well as via the deductions of the intricate molecular modeling undertaken.

Oscillatory studies highlighted that the hydrogel systems (SRHS) employed to form the inner and outer BPM of the I^3 exhibited stimulus-responsive rheological behavior on exposure to and removal of the inflammatory environment. The average loss tangent was highest when exposed to inflammatory conditions. FTIR highlighted that the final crosslinked BPMs showed the presence of bands inherent to all its components, with a reduction in intensity of selected bands and the appearance of new bands, attributable to the intra- and intermolecular crosslinking instigated in the presence of the chemical crosslinkers and initiators, namely DCC and NHS in the outer core and gluteraldehyde in the inner core. Overall, there was a significant shift in the T_g in the I^3, represented as the outer and inner BPM, compared to the native components, indicative of the high degree of crosslinking within the

I^3. The I^3 formulation displayed adequate responsive capabilities on exposure to and removal of the inflammatory stimulus in terms of drug release. Ciprofloxacin was released to a greater extent due to its presence in the outer BPM, which is anticipated to erode at a faster rate, as well as its non-incorporation in a nano-carrier. MRI highlighted that fluid ingress with device hydration and gelling can be considered as a significant predictor of the drug release profiles of the I^3 with the minimal change in the device area (which had a high degree of gelling) showing a notable negative correlation with both indomethacin and ciprofloxacin release under normal conditions ($R^2 = -0.8856$, and $R^2 = -0.8783$, respectively). However, under inflammatory conditions, there was a notable decrease in the area of the I^3, which exhibited a comparatively lower degree of hydration and gelling. This correlated positively and significantly with the observed drug release of both indomethacin and ciprofloxacin ($R^2 = 0.9695$ and 0.9888, respectively). Image analysis of erosional behavior visualized via SEM indicated a significant shift towards a more porous structure of both the inner and outer BPM on exposure to an inflammatory environment.

Physicochemical and physicomechanical characterization undertaken was therefore essential for delineating *in vitro* attributes for predicting the *in vivo* performance of the device, with specific reference to its inflammation-responsive transitions. Ultimately, preliminary *in vivo* studies highlighted that *in vitro* stimulus-responsiveness translated into enhanced drug release in the inflamed rabbit eye *in vivo*, with an observed reduction in the level of intraocular inflammation. The I^3 demonstrated successful bioresponsive attributes *in vitro* and, in the preliminary stages, *in vivo*, and could potentially improve patient outcomes in posterior segment inflammatory disorders.

REFERENCES

1. Herrero-Vanrell R, Refojo MF. Biodegradable microspheres for vitreoretinal drug delivery. Adv Drug Deliv Rev. 2001;52(1):5–16.
2. Del Amo EM, Urtti A. Current and future ophthalmic drug delivery systems: a shift to the posterior segment. Drug Discov Today. 2008;13(3–4):135–43.
3. Alvarez-Lorenzo C, Concheiro A. Molecularly imprinted polymers for drug delivery. J Chromatogr B. 2004;804(1):231–45.
4. Barbu E, Verestiuc L, Nevell TG, Tsibouklis J. Polymeric materials for ophthalmic drug delivery: trends and perspectives. J Mater Chem. 2006;16:3439–43.
5. Panyam J. Inflammation-responsive drug delivery system. Pharmaceutical Sciences, WSU__.htm. Available from: http://research.wayne.edu/idre/db/?view=person&id=42. Relocated in part to: http://research.wayne.edu/idre/tools/faculty-interests.php?id=70.
6. Ahn BJ, Moshfeghi AA. Implantable Posterior Segment Drug Delivery Devices. Ophthalmology Web; 2008. Available from: http://www.ophthalmologyweb.com/Spotlight.aspx?spid=23&aid=253&headerid=23.
7. Thilek Kumar M, Pandit JK, Balasubramaniam J. Novel therapeutic approaches for uveitis and retinitis. J Pharm Pharm Sci. 2001;4(3):248–54.
8. Allergan Inc. EP1750688—Steroid intraocular implants having an extended sustained release for a period of greater than 2 months; 2007. Available from: https://register.epo.org/espacenet/application?number=EP05744945.
9. Saliba JB, Gomes Faraco AA, Yoshida MI, de Vasconcelos WL, da Silva-Cunha A, Mansur HS. Development and characterization of an intraocular biodegradable polymer system containing cyclosporine A for the treatment of posterior uveitis. Mat Res. 2008;11(2):207–11.
10. Barcia E, Herrero-Vanrell R, Díez A, Alvarez-Santiago C, López I, Calonge M. Downregulation of endotoxin-induced uveitis by intravitreal injection of polylactic-glycolic acid (PLGA) microspheres loaded with dexamethasone. Exp Eye Res. 2009;89:238–45.
11. Haesslein A, Hacker MC, Ueda H, Ammonb DM, Borazjani RN, Kunzler JF, *et al*. Matrix modifications modulate ophthalmic drug delivery from photo-cross-linked poly(propylene fumarate)-based networks. J Biomat Sci. 2009;20:49–69.
12. Ligório Fialho S, Behar-Cohen F, Silva-Cunha A. Dexamethasone-loaded poly(ε-caprolactone) intravitreal implants: a pilot study. Eur J Pharm Biopharm. 2008;68(3):637–46.
13. Holekamp NM, Thomas MA, Pearson A. The safety profile of long-term, high-dose intraocular corticosteroid delivery. Am J Ophthalmol. 2005;139(3):421–8.
14. Zeimer R, Goldberg MF. Novel ophthalmic therapeutic modalities based on noninvasive light-targeted drug delivery to the posterior pole of the eye (Drug Delivery to the Posterior Segments of the Eye). Adv Drug Deliv Rev. 2001;52(1):49–61.
15. Hawkins CL, Davies MJ. Direct detection and identification of radicals generated during the hydroxyl radical-induced degradation of hyaluronic acid and related materials. Free Radical Biol Med. 1996;21:275–90.
16. Zhao XB, Fraser JE, Alexander C, Lockett C, White BJ. Synthesis and characterisation of novel double crosslinked hyaluronan hydrogel. J Mater Sci Mater Med. 2002;13:11–6.
17. Saltzman WM. Drug delivery: engineering principles for drug therapy. Oxford: Oxford University Press; 2001.
18. Hermanson T. Bioconjugate Techniques. 2nd Ed. London: Elsevier; 2008. P. 220.
19. Choonara YE, Pillay V, Ndesendo VMK, du Toit LC, Kumar P, Khan RA, *et al*. Design of polymeric nanoparticles by synthetic wet chemical processing strategies for the sustained delivery of anti-tuberculosis drugs. Coll Interf B Biointerface. 2011;87:243–54.
20. Warhurst DC, Craig JC, Adagu IS, Meyer DJ, Lee SY. The relationship of physico-chemical properties and structure to the differential antiplasmodial activity of the cinchona alkaloids. Malar J. 2003;2:26.
21. Pearlman DA, Case DA, Caldwell JW, Ross WS, Cheatham TE, DeBolt III S, *et al*. AMBER, a package of computer programs for applying molecular mechanics, normal mode analysis, molecular dynamics and free energy calculations to simulate the structural and energetic properties of molecules. Comp Phys Commun. 1995;91:1–41.
22. Yu BY, Chung JW, Kwak S-Y. Reduced migration from flexible poly(vinyl chloride) of a plasticizer containing β-cyclodextrin derivative. Environ Sci Technol. 2008;42:7522–7.
23. Herh P, Tkachuk J, Wu S, Bernzen M, Rudolph B. The rheology of pharmaceutical and cosmetic semisolids. ATS RheoSystems. 1998:12–14.
24. Takka S. Propranolol hydrochloride—anionic polymer binding interaction. Il Farmaco. 2003;58(10):1051–6.
25. Nielson LE. Mechanical properties of polymers and composites, vol. 1. New York: Marcel Dekker; 1974.

26. Yui N, Nihira J, Okano T, Sakurai Y. Inflammation responsive degradation of crosslinked hyaluronic acid gels. J Control Release. 1992;22:105–16.
27. Tajiri T, Morita S, Sakamoto R, Suzuki M, Yamanashi S, Ozaki Y, *et al*. Release mechanisms of acetaminophen from polyethylene oxide/polyethylene glycol matrix tablets utilizing magnetic resonance imaging. Int J Pharm. 2010;395(1–2):147–53.
28. Shaikh RP, Kumar P, Choonara YE, du Toit LC, Pillay. Crosslinked electrospun PVA nanofibrous membranes: elucidation of their physicochemical, physicomechanical and molecular disposition. Biofabr. 2012;4(025002):doi 10.1088/1758-5082/4/2/025002.
29. Koura Y, Fukushima A, Nishino K, Ishida W, Nakakuki T, Sento M, *et al*. Inflammatory reaction following cataract surgery and implantation of acrylic intraocular lens in rabbits with endotoxin-induced uveitis. Eye (Lond). 2006;20(5):606–10.
30. Cheruvu NP, Ayalasomayajula SP, Kompella UB. Retinal delivery of sodium fluorescein, budesonide & celecoxib following subconjunctival injection. Drug Dev Deliv. 2003;3(6):posted on: 3/28/2008.
31. Kobayashi A, Naito S, Enomoto H, Shiomoi T, Kimura T, Obata K, *et al*. Serum levels of matrix metalloproteinase 3 (stromelysin 1) for monitoring synovitis in rheumatoid arthritis. Arch Path Lab Med. 2007;131(4):563–70.
32. Tian Y, Li Y, Xu X, Jin Z, Jiao A, Wang J, *et al*. A novel size-exclusion high performance liquid chromatography (SE-HPLC) method for measuring degree of amylose retrogradation in rice starch. Food Chem. 2010;118:445–8.
33. Xie YH, Soh AK. Investigation of non-covalent association of single-walled carbon nanotube with amylose by molecular dynamics simulation. Mat Lett. 2005;59(8–9):971–5.
34. Hoare TR, Kohane DS. Hydrogels in drug delivery: progress and challenges. Polymer. 2008;49:1993–2007.
35. Tammi MI, Day AJ, Turley EA. Hyaluronan and homeostasis: a balancing act. J Biol Chem. 2002;277(7):4581–4.
36. Mlčochová P, Bystrický S, Steiner B, Machová E, Koóš M, Velebný V, *et al*. Synthesis and characterization of new biodegradable hyaluronan alkyl derivatives. Biopolymers. 2006;82(1):74–9.
37. Magnani A, Rappuoli R, Lamponi S, Barbucci R. Novel polysaccharide hydrogels: characterization and properties. Polym Adv Tech. 2000;11(8–12):488–95.
38. Beppu MM, Vieira RS, Aimoli CG, Santana CC. Crosslinking of chitosan membranes using glutaraldehyde: effect on ion permeability and water absorption. J Membr Sci. 2007;301(1–2):126–30.
39. Kildeeva NR, Perminov PA, Vladimirov LV, Novikov VV, Mikhailov SN. About mechanism of Chitosan cross-linking with glutaraldehyde. Russ J Bioorg Chem. 2009;35:360–9.
40. Yui N, Nihira J, Okano T, Sakurai Y. Regulated release of drug microspheres from inflammation responsive degradable matrices of crosslinked hyaluronic acid. J Control Release. 1993;25(1–2):133–43.